1970

Penetration in granite by shaped charge liners of various metals

Hemendra Nath Kalia

PENETRATION IN GRANITE BY SHAPED CHARGE LINERS OF VARIOUS METALS

by

HEMENDRA NATH KALIA, 1939

A DISSERTATION

Presented to the Faculty of the Graduate School of the

UNIVERSITY OF MISSOURI-ROLLA

In Partial Fulfillment of the Requirements for the Degree

DOCTOR OF PHILOSOPHY

in

MINING ENGINEERING

1970

Ronald R. Rollins
(Advisor)

George B. Clark

D. S. Wolf

James J. Scott

B. Gillett

ABSTRACT

The penetration in Missouri red granite by cylindrical charges with metal liners of aluminum 2011 (T-3), aluminum 7075 (T-6), yellow brass, monel, maraging steel (vascomax 250), and copper was measured. Metals having high ductility and moderate compressive strength penetrated deeper than high strength maraging steel. Aluminum required a greater standoff for optimum penetration than the other metal liners tested.

Preliminary metallographic studies of the liner metals and slugs showed that the grains had elongated along the slug axis. The metals containing zinc formed very small or no slugs.

The granite grains were highly fractured. The holes were discolored and coated with jet metal. Penetration was affected by bedding planes and joints in the rock.

Jet characteristics could not be photographed using a high speed framing camera because the view was obscured by the luminous front created by shock waves. Jet tip velocities were measured by pin oscilloscope techniques and were in the range of 7.91 - 9.83 millimeters per microsecond. The rate of penetration in granite was also obtained in this same manner.

A mathematical expression was developed to calculate collapse time of cones using three-dimensional collapse criteria.

ACKNOWLEDGMENT

The author considers it a privilege to express his gratitude to Dr. R. R. Rollins and Dr. G. B. Clark for their invaluable support and suggestions throughout this investigation.

He is also grateful to E. I. Dupont De Nemours Company, and the United States Government, Department of Defense, for their financial support under fund number DACA-45-69-C-0087.

Sincere thanks are extended to Dr. J. B. Clark, Dr. W. A. Frad, Mr. S. Vora and Mr. S. G. Bankar for their help in obtaining metallographs; to Dr. E. L. Bertrand for his help in measuring slug densities; and to Dr. C. J. Haas for his assistance in calibrating the pin oscilloscope for velocity measurements.

He is grateful to Mr. B. Hale for machining the liners, to Mr. E. Rapier, and Mr. E. Packheiser, for their aid in performing the experiments.

Finally he extends his appreciation to his parents for their patience and thoughtfulness throughout his study period.

TABLE OF CONTENTS

LIST OF ILLUSTRATIONS

LIST OF TABLES

I. INTRODUCTION

A. General

The term "shaped charges" is generally applicable to explosive charges with lined or unlined cavities formed at the end opposite to the point of initiation. The unlined cavity effect is known as the Munroe effect in the United States and the United Kingdom (1), the Neumann effect in Germany, and the Cumulation effect in Russia (2).

There is no evidence that Munroe or Neumann discovered the lined-cavity effect, which is a phenomenon quite different from the unlined-cavity effect. Baum (2) has credited Sukhreski with the systematic investigation of the cumulation effect. Eichelberger (3) credits R. W. Wood with the recognition in 1936 of the usefulness of metallic liners in the hollowed charges to produce fragments of extremely high velocity.

Fundamental and developmental studies as well as the design of shaped charge weapons were simultaneously undertaken by Dupont's Eastern laboratories and by Kistiakowsky, Taylor, MacDougal, Jacobs, and others in 1941.

This study was undertaken to determine the penetrability of shaped charge jets into granite. This was accomplished by using metallic liners and composition C-4 as the high explosive.

Shaped charges have found extensive use in military applications. The industrial uses are limited to oil well casing perforations, furnace tapping, and linear cutting charges.

Lined cavity charges were investigated by Clark (4), Austin (5),

and Huttl (6), to evaluate their effect in breaking concrete, rhyolite, and limestone boulders. From the literature research it appears that no systematic investigation has been made to evaluate shaped charges for drilling and blasting of rock. The ability of shaped charges to form high velocity jets makes them interesting for this application.

B. Nature of the Investigation:

The primary objective of this study was to evaluate the penetrating capability of shaped charges fabricated from various liner metals on rocks. This was accomplished by investigating the following: six different liner metals; change in the physical properties of the liners by annealing; behavior of rock under jet impact; and jet parameters, formation, and penetration theory.

A large volume of information is available on the penetration of metallic targets by metallic jets. The first order penetration law was developed independently by Pack, Mott, and Hill (7), Pugh (1), and Pack and Evans (8, 9) applying the Bernoulli theorem. The total penetration is given by:

$$P = L\,(\rho_j/\rho_t)^{\frac{1}{2}} \qquad (1)$$

Equation (1) holds only for ideal jets and for targets with zero yield strength as compared to the pressure of the jet. Thus, one expects variation from this law. It is observed that the resistance to penetration in rock is due not only to the density of the jet and the jet length, but to other factors as well, e.g.; the joints, bedding planes, and anisotropic nature of the target.

II. THEORY OF JET FORMATION AND PENETRATION

The classical two-dimensional theory of jet formation (8, 10) has been modified (3) to account for the jet tip velocity gradient. The modified two-dimensional theory visualizes the liner being collapsed upon itself by the pressure of the detonation products. As the pressure is applied progressively to the liner, it collapses upon the axis at an angle (Figure 1). This collapse angle is greater than the apex angle of the cone.

The two dimensional theory and other similar theories neglect the acceleration of the coordinate of the stagnation point and the thickening of the liner. In order to account for these parameters one requires the solution of a three-dimensional time dependent problem.

A. Theory of Cone Collapse and Jet Formation:

The analytical technique used for collapsing cylindrical shells (11) may be applied to collapsing conical liners. According to this theory, when an undisturbed cylindrical shell contracts the velocity of the outer surface would tend to diminish and the inner velocity should increase (Figure 1). As an initial approximation, it is assumed that the liner material is incompressible and that the wall moves inward normal to the original surface of the cone.

For a cone of half apex angle α (Figure 2) the kinetic energy of the thin element of unit thickness can be obtained by considering the section to collapse along the slant height of the cone AB. The kinetic energy of this element is

$$T = \rho\pi \mathrm{Cos}\alpha \, (S_3\dot{S}_3)^2 \ \ln \ S_2/S_3 \ . \quad (2)$$

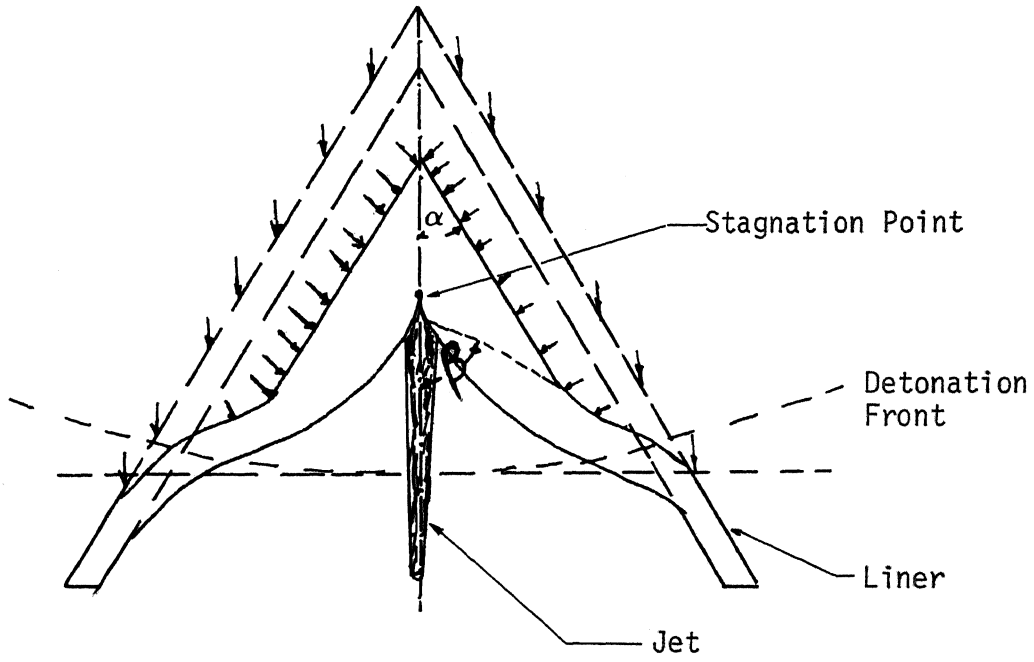

Figure 1. Cone Collapse and Jet Formation

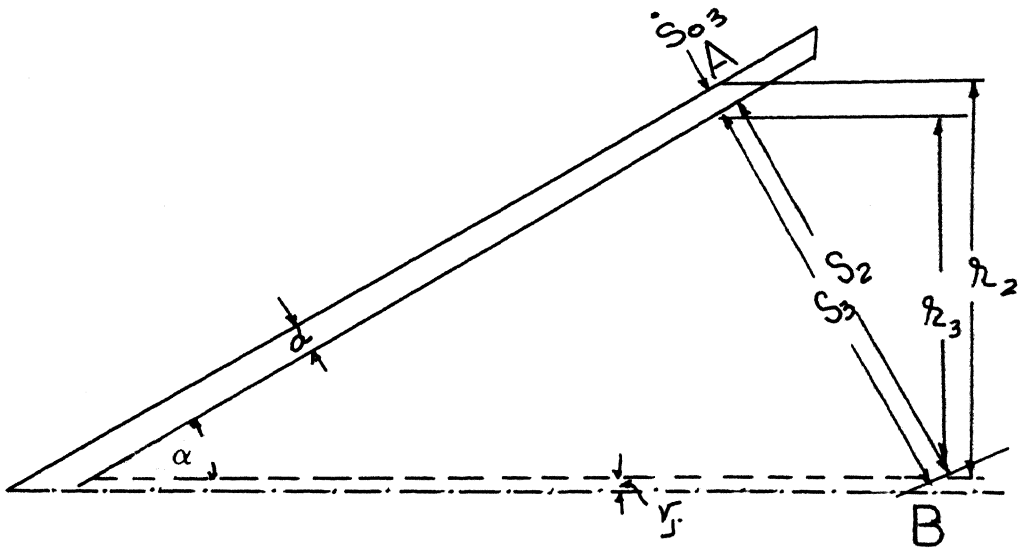

Figure 2. Cone Collapse Dimensions

or the time of collapse is given by

$$t_c = (\rho\pi\Delta 1\ \mathrm{Cos}\alpha/T)^{\frac{1}{2}} \quad 1/2 \int_{r_j/\mathrm{Cos}\alpha}^{S_{3i}} S_3 \ln\left(\frac{S_3 + d}{S_3}\right) dS_3 \quad . \quad (3)$$

Equation (3) was numerically integrated for successive values of S_{3i} and the time of collapse was determined for a constant collapse velocity. Figure 3 shows that for a constant jet radius the movement of the stagnation point is constant. This partially explains why the two-dimensional theory offers such a good approximation for a three-dimensional process. Modifications similar to those employed by Eichelberger (12) and Jackson (13) will undoubtedly give a truer picture of jet formation and of the actual process involved.

B. Theory of Jet Penetration:

The basic theory of penetration by high-speed metallic jets was developed using Bernoulli's theorem (Equation 1).

Various authors have modified this equation with empirical constants to explain penetration of various types of metallic targets. This equation does not take into account the jet velocity and target strength. Dipersio (14) has modified the equations developed by Allison and Vitali (15), and the concept of this theory (14) treats three cases: a. continuous jet, b. partially continuous jet, and c. completely broken jet. The total penetration for these three conditions is given by equations 4-6.

$$P_T = Z_o \left[V_j^{o}/(1 + \gamma)\ U^{min} \right]^{1/\gamma} - 1 \qquad (4)$$

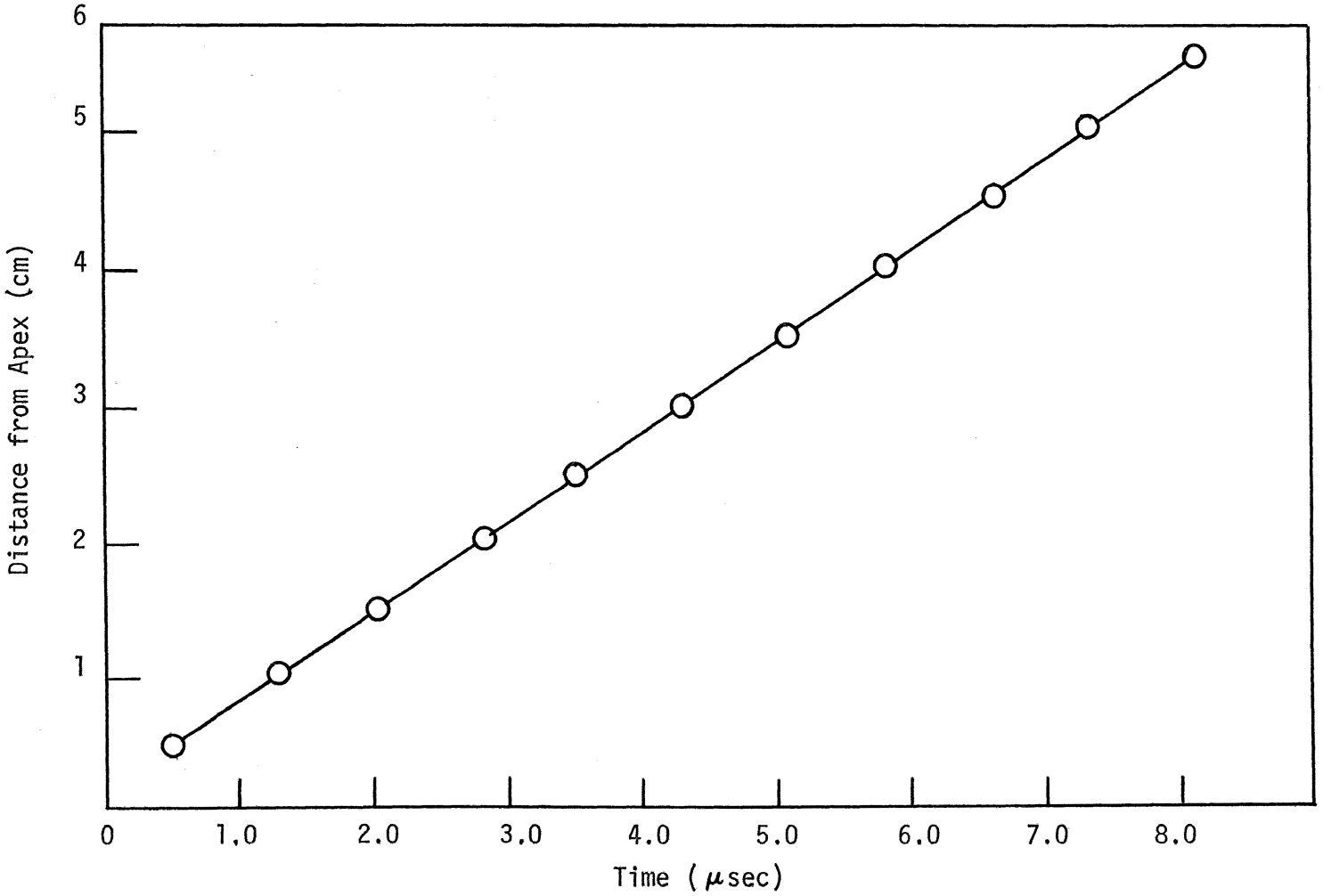

Figure 3. Collapse Time for 60 Degree Liners

$$P_T = \frac{(1+\gamma)\,(v_j{}^o t_1)^{1/(1+\gamma)} Z_o{}^{\gamma/(1+\gamma)}}{\gamma} - \frac{\sqrt{(1+\gamma)\,U^{min}\,t_1 (v_j{}^o t_1)^{1/(1+\gamma)} Z_o{}^{\gamma/(1+\gamma)}}}{\gamma} - Z_o \qquad (5)$$

$$P_T = \frac{V_j{}^o t_1 - \sqrt{U^{min}\,t_1\,(V_j{}^o t_1 + \gamma Z_o)}}{\gamma} \qquad (6)$$

The basic assumptions in the development of equations (4), (5), and (6) are that the target and jet are incompressible, the jet originates at a distance Z_o from the target, the jet breaks up axially into individual particles simultaneously throughout its entire length, and all particles above a critical velocity for a particular target contribute to penetration.

For a given charge and target the penetration increases linearly with Z_o for a continuous jet (Equation 4). The penetration increases with jet tip velocity and with a decrease in U^{min}. The minimum penetration velocity, U^{min}, for a target can be determined experimentally. The jet tip velocity is a function of liner and explosive properties. Equation 4 is applicable to the penetration by a continuous jet.

Maximum penetration is obtained at the upper limit of application of equation (6), which defines the penetration for a partially contin-

uous jet. The maximum penetration is given by

$$P_{max} = \sqrt{\frac{\rho_j}{\rho_t}} \left[v_j^o - \sqrt{U^{min} \left(V_j^o + \gamma \frac{Z_o}{t_1} \right)} \right] \qquad (7)$$

for a given liner and target.

Maximum penetration is obtained for high jet tip velocity and optimum jet breakup time, t_1. This equation explains why high velocity explosives and high density cohesive jets produce the maximum target penetration.

III. EXPERIMENTAL DESIGN

A. Design of Shaped Charges

A concise summary of shaped charge design is given by Klamer (16). For this investigation the following design parameters were considered:

1) Liner material
2) Apex angle
3) Liner thickness
4) Charge dimensions
5) Type of explosive
6) Target material

1. Liner material

Zernow (17) tested various metals for shaped charge liners and arrived at the conclusion that copper, nickel, aluminum, and silver (all face centered cubic) behave in a similar manner with few noticeable differences between them. These metals behave in a ductile fashion in the dynamic Bridgman region and stretch in a taffy-like manner in the flight phase. Copper is the most effective liner material for metal targets because of its ductility and density.

Iron (body centered cubic) and all 1020 mild steels showed high ductility in the dynamic Bridman region but fractured in relatively large fragments shortly after leaving the high pressure region.

The hexagonal metals tested by Zernow (17) show distinct characteristics. In the flight phase the jets from these metals break up into fine fragments. Magnesium shows a ductile nature in the dynamic Bridgman region while cobalt shows anomalous behavior.

Metals under higher pressures (21,000-31,500 kg/cm^2) show a different degree of elongation than they do under ambient pressures. The amount of energy imparted to the plastic flow and fracturing changes as the pressure is increased (18), hence the mode of liner failure will change with the applied pressure.

Metals having low melting points, cadmium (hexagonal), zinc (hexagonal), lead (face centered), and tin (tetragonal), all behave in a unique manner despite the diversity in their crystal structure. It appears that for those having melting points $\geq 625^{o}C$ the crystal structure correlates with the observed behavior of the jet, whereas in low melting point metals, $460^{o}C \leq T \leq 625^{o}C$, the low melting point itself appears to be best correlated with the behavior of the jet.

The metals selected for this investigation are presented in Table 1 with their physical properties.

2. Apex angle:

Conical liners were used in this study because they are easy to machine and have proven to be of an effective geometry. Brimmer (19) has shown that for metallic targets the optimum cone angle for maximum penetration is approximately 60^{o}. This cone angle was used in this study.

3. Liner thickness:

The liners were designed with optimum liner thickness (l_{th} optimum). This thickness was obtained by using the relationship suggested by Winn (20).

$$l_{th}\ \text{Optimum} = \frac{(l_{th}\ \text{Optimum Copper})\ (\text{Density of Copper})}{(\text{Density of Metal})} \qquad (8)$$

Table 1

Physical Properties of Liner Metals

Metal Type	Tensile Strength $kg/cm^2 \times 10^3$	Compressive Strength $kg/cm^2 \times 10^3$	Elongation Percent	Hardness Rockwell	Modulus of Elasticity $kg/cm^2 \times 10^5$	Modulus of Rigidity $kg/cm^2 \times 10^5$	Metal Density gm/cm^3	Melting Point ^oC
Aluminum T-3, 2011	3,866	3.023	15	95E	7.171	2.671	2.82	535-643
Aluminum T-6, 7075	5,835	5.132	17	100E	-----	2.742	2.80	476-637
Brass (yellow)	4.288	3.515	23	84K	7.382	2.742	8.47	904.4
Monel	6.679	5.273	27	96B	18.279	6.679	8.84	1300.0
Maraging Steel Vascomax 250	9.8	10.43	19	29C	18.55	7.14	8.0	------
Copper	2.39	----	45-50	34RE	11.95	-----	8.96	1083.0

Percentage Composition of the Metals

Aluminum T-3	Al 93.5%, Cu 5.5% Pb 0.5%, Bi 0.5%
Aluminum T-6	Al 91.2%, Zn 5.5%, Mg 2.5%, Cu 1.5%, Cr 0.3%
Yellow Brass	Cu 65%, Zn 35%
Monel	Ni 66.26%, Cu 31.26%, Fe 1.12%, Al 0.12%, Si 0.7%, C .19%, Mn 0.94%
Steel	Ni 18.5%, Co 7.5%, Mo 4.8%, Fe 68.37%, others 0.82%
Copper	Cu +99%

The optimum thickness of the copper liner was taken as 0.105 cm.

The average weights and thickness of the 60 degree liners tested were:

Metal	Weight (gm)	Liner thickness (cm)
Aluminum 2011 (T-3)	32.5 ± 0.25	0.3500 ± 0.002
Aluminum 7075 (T-6)	32.0 ± 0.25	0.3480 ± 0.002
Yellow Brass	36.1 ± 0.25	0.1150 ± 0.002
Maraging Steel	34.7 ± 0.25	0.1161 ± 0.002
Monel	34.2 ± 0.25	0.1065 ± 0.002
Copper (42 Degree)	47.9 ± 1.00	0.1050 ± 0.002

4. Charge Dimensions:

The charge length must be sufficient to provide a fully developed detonation front before the front makes contact with the liner. Baum (2) points out that the minimum height of the charge for which its active portion attained its limiting value for a cylindrical charge is equal to $H_{lim} = CR + h$. Thus, H_{lim} for conical liners is approximately equal to 2 cone diameters. Framing camera photographs show that the detonation front is fully developed when it contacts the cone for a charge length of 2 cone diameters. Based on these observations and the literature review a charge length of 2 cone diameters was used, which in the present investigation equalled 10 cm. The charge to cone diameter ratio was 1.04.

5. Type of explosive:

The characteristics of the explosives most commonly used for shaped

charge studies are presented in Table 2. The most desirable properties are high detonation pressure and velocity. Composition C-4 (Table 3) was used in this study because it possesses these features and is also easy to load. The charges were loaded at a density of 1.6 gm/cc at which this explosive has a theoretical velocity of 8611 m/sec and a pressure of 327,069 kg/cm^2.

A mechanical device was used to ensure uniform loading of the explosive charges and a number 8 blasting cap was adequate for detonating the composition C-4.

6. Target material (Table 4):

Initial tests were performed on cast concrete blocks (Table 5) and rhyolite (Table 6). These targets failed in radial strain. It was not possible to obtain hole dimensions. Missouri red granite was used as the target material for the latter part of this study.

Table 2 (Ref. 19)

Shaped-Charge Explosives

Designation	Loading Density g/cc 25°C	Detonation Velocity Meters Per Sec	Relative Power*	Impact Sensitivity**	Stability***	Remarks
Cast Pentolite 50/50	1.65	7,500	126	12	moderately stable	Used chiefly in shaped charges; penetration is 90-95% that of 65/35 Cyclotol. More sensitive than 65/35 Cyclotol.
Cast Cyclotol 65/35	1.71	7,995	134	--	fairly stable	Better for filling small shaped charges.
Cyclotol 70/30	1.725	7,790	135	14	fairly stable	One of the most effective shaped charge explosives; too viscous to load small shaped charges.
Cast RDX	1.65	8,180	150	8	fairly stable	Samples stored 2.5 yr. at ordinary temp. found to be perfect. Germans used pressed pre-formed pellets in shaped charges (Comp. A: RDX 90% wax 10%); not used alone in shaped charges.
Cast Comp. B	1.88	7,840	133	14	very stable	About 20% more effective than cast TNT; high shaped charge efficiency; good loading characteristics; sensitive to shock.

Table 2 (cont'd)

Shaped-Charge Explosives

Designation	Loading Density g/cc 25°C	Detonation Velocity Meters Per Sec	Relative Power*	Impact Sensitivity**	Stability***	Remarks
Plastic Comp. C-2 (DuPont)	1.57	7,660	126	--	--	Hardens when stored at elevated temperature.
Plastic Comp. C-3	1.60	7,625	126	14	moderately stable	Comp. C modified to provide a good explosive for molded and shaped charges; tends to harden in storage; special packaging needed to prevent exudation even at 55°F.
Plastic C-4	1.59	8,578	130	19	stable	Composition C-4 has been developed to improve the instability and hygroscopy of C-3. Will not undergo exudation at 77°C.
Castable, similar to Comp. B PTX-2	1.70	8,065	138	--	stable	Developed by Picatinny Arsenal as castable filling for shaped charges.
Small charges pressed; medium & large charges, cast TNT	1.56 cast 1.56 pressed	6,640 6,825	100	14-15	very stable	Used for blasting, demolition.

Table 2 (cont'd)

Shaped-Charge Explosives

Designation	Loading Density g/cc 25°C	Detonation Velocity Meters Per Sec	Relative Power*	Impact Sensitivity**	Stability***	Remarks
Cast HBX	1.65	7,100	113	8	stable	Intended as replacement for Torpex in depth bombs; generation of hydrogen may deform cavity.
Cast Torpex 2	1.71	7,200	116	6	very stable	Mainly used in underwater ordnance; generation of hydrogen may deform cavity.
Astrolite G Liquid	1.4	8,600	174	--	--	Has a very high gas volume. Suitable for shaped charges and fragment acceleration.
Astrolite A-1-5 Liquid	1.6	7,500	237	--	--	It is a white explosive and melts at 273° - 280°C. It is very similar to cyclonite in sensitivity, brisance and strength.
Cast HMX	1.84	9,124	150	9	--	

*Power of an equal volume of explosive relative to TNT (= 100) based on the ballistic mortar.
** Picatinny Arsenal apparatus
*** Those classified as moderately stable will survive all but drastic tropical storage; stable and very stable will survive this.

Table 3

Properties of Composition C-4

Composition C-4	Percentage	Empirical Formula	Heat of Formation Kcal/Mole
RDX	91.0	$C_3H_6N_6O_6$	-18.3
Polyisobutylene	2.1	C_4H_8	-19.7***
Motor Oil (SAE 10)	1.6	CH_2	- 4.9
Di-(2-ethylhexyl) Sebacate	5.3	$C_{26}H_{50}O_4$	-306.9***
	100.0		
Empirical formula for C-4		$C_{1.80}H_{3.60}N_{2.46}O_{2.50}$	
Heat of formation for C-4		- 126.1 Kcal/mole	
Heat of reaction for C-4*		983 cal/g	

Using this information, a loading density of 1.59 g/cm^3, and the B. K. W. equation of state, the following information was obtained by computer calculations.**

Density	1.59 g/cm^3
Detonation velocity	8,578 m/sec
Particle velocity	2,320 m/sec
Sound velocity	6,258 m/sec
Detonation pressure	312,333 atm
Detonation temperature	3,374^{o}k
Total gas	34.667 moles/kg of explosives
Total solid (carbon)	12.176 moles/kg of explosive

*Experimental value from oxygen bomb calorimeter measurements, personal communication from personnel at Picatinny Arsenal.

**Operator's Manual for Ruby UCRL 6815 or TID 4500.

***Personal communication from Dr. D. S. Wulfman

Table 4

Physical Properties of Target Materials

Rock Type	Density g/cc	Impact Hardness	Compressive Strength $g/cm^2 x10^4$	Compression Wave Velocity $cm/sec\ x10^5$	Apparent Porosity %
Concrete	2.069	31*	84.0	4.45*	18.69
Rhyolite	2.620	---	337.0	-----	0.16
Missouri Red Granite	2.60	53*	119.0	4.52*	0.4

*Reference (21)

Table 5

Penetration in Concrete by 60^{o} Liners

Charge No.	Liner Thickness cm	Standoff cm	Penetration cm
35 S	0.1161	20.0	22.5
36 S	0.1161	15.0	38.5
37 S	0.1161	5.0	31.5
38 S	0.1161	10.0	17.5
49 A16	0.3480	15.0	39.6
50 A16	0.3480	20.0	22.8
53 A16	0.3480	15.0	35.5

S Maraging Steel (Vascomax 250)

A16 Aluminum 7075 (T-6)

Table 6

Penetration in Rhyolite by 60 Degree Liners

Charge No.	Liner Thickness cm	Standoff cm	Penetration cm
42 B	0.115	5.0	10.0
43 B	0.115	10.0	20.0
44 B	0.115	17.5	15.0
45 B	0.115	29.0	22.5
52 A16	0.348	20.0	10.0
54 A16	0.348	15.0	10.0

B Yellow Brass

A16 Aluminum 7075 (T-6)

IV. EXPERIMENTAL WORK AND RESULTS

A. Penetration Studies:

Penetration depths were measured by using a graduated metallic probe. The probe was inserted into the hole to gage the penetration ignoring the spalled depth. The hole was assumed to be a right circular cone, and the diameter was measured along the transverse axis. The spalled depth was measured as accurately as possible. The hole was plotted to scale and the slant edges were extended to the base of the spalled surface. The radius so obtained was taken as the effective radius of the hole. An expendable template was designed to centrally locate the detonator and produce a symmetrical detonation front (Figure 4).

Charges were fired at various standoffs (Figure 1C) to obtain the the optimum standoff (Table 7) for liner metals used. This standoff was used to measure the rate of penetration through granite blocks and penetration by liners having 42, 55, and 75 degree apex angles (Table 8).

1. Penetration Results:

Figure 5 (Table 9): Penetration in granite by aluminum 2011 (T-3).

This metal showed considerable variations in penetration. This may be attributed to the compressive strength of the metal, which was less than any other metal tested. The 42, 55, and 75 degree liners gave less penetration than the 60 degree liners. One of the liners was annealed for 20 hours at 413^{o}C. Penetration by the annealed liner was less than that for non-annealed liners. The maximum penetration was obtained at a standoff of 20.0 cm (4.0 cone diameters).

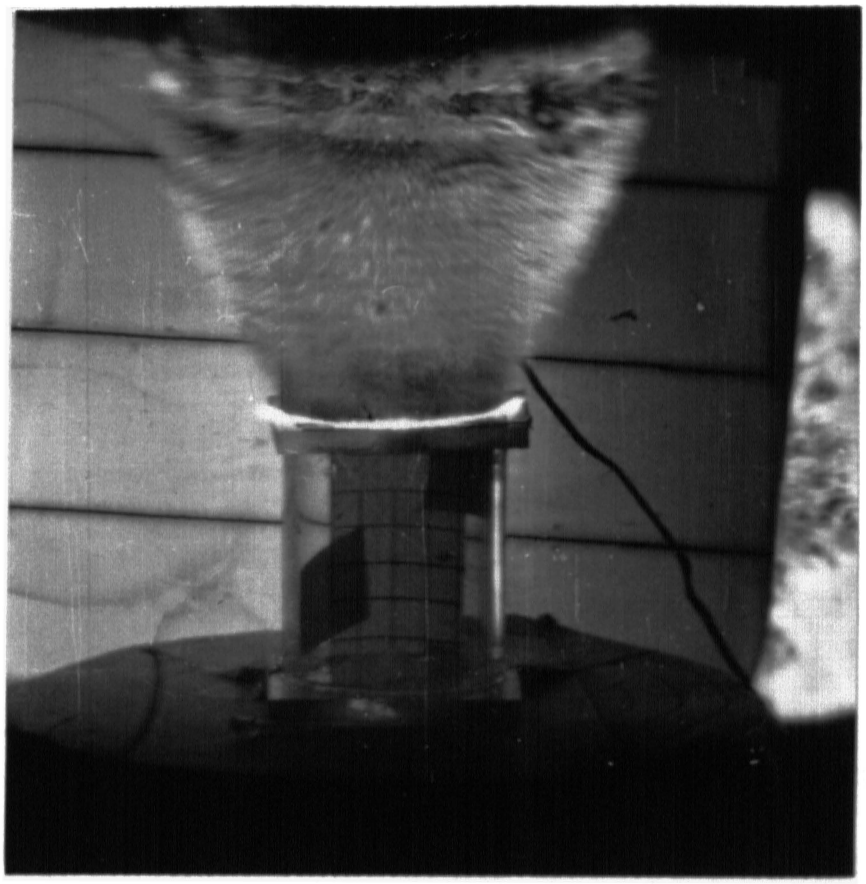

Figure 4. Fully developed detonation front 28 μ secs after initiation

Table 7

Optimum Standoff

Aluminum 2011 (T-3)	20.0	cm or	4.0	CD
Aluminum 7075 (T-6)	22.5	cm or	4.5	CD
Yellow Brass	15.0	cm or	3.0	CD
Monel	17.5	cm or	3.5	CD
Maraging Steel	10.0	cm or	2.0	CD
Copper (42 degree)	16.25	cm or	3.25	CD

Table 8

Penetration in Granite by Various Liners Tested at the Optimum andoff for 60° Liners.

arge .	Apex Angle deg.	Liner Thickness cm	Stand off cm	Penetration cm	Hole Radius cm	Hole Volume cc
5 T3	42	0.2750	20.0	10.1	-	+
L T3	55	0.2750	20.0	9.3	3.5	119.3[c]
7 T3	60	0.3500	20.0	15.0	-	+
4 T3	75	0.3160	20.0	9.9	1.2	14.93
' T6	42	0.2750	22.5	12.2	0.9	10.35
: T6	55	0.2750	22.5	11.1	0.5	5.70
T6	60	0.3480	22.5	13.2	-	-
T6	75	0.3160	22.5	9.1	-	-
M	42	0.1000	17.5	12.7	1.3	11.3
M	55	0.1000	17.5	12.3	0.7	6.3
M	60	0.1065	17.5	17.0	1.8	15.6
M	75	0.1000	17.5	9.7	0.9	8.2
B	42	0.1000	15.0	11.5	1.3	11.3
B	55	0.1000	15.0	15.3	0.8	6.3
B	60	0.1150	15.0	17.4	1.7	26.2
B	75	0.1500	15.0	13.9	0.9	22.5
S	42	0.1000	10.0	11.8	0.7	6.0
S	55	0.1000	10.0	11.7	1.1	14.8

Table 8 (continued)

Penetration in Granite by Various Liners Tested at the Optimum Standoff for 60^{o} Liners.

Charge No.	Apex Angle deg.	Liner Thickness cm	Stand off cm	Penetration cm	Hole Radius cm	Hole Volume cc
40 S	60	0.1161	10.0	16.0	1.5	37.7
30 S	75	0.1500	10.0	8.0	0.7	4.1

\+ = Crater (No hole radius could be measured)

T3 = Aluminum 2011 (T3)

T6 = Aluminum 7075 (T6)

M = Monel

B = Brass

S = Steel

C = Crater

G = From graph

Figure 6 (Table 10): Penetration in granite by aluminum 7075 (T-6).

A gradual increase in penetration can be seen from 4.0 to 4.5 cone diameters. Penetration by 42, 55, and 75 degree liners when fired at the best standoff for 60 degree liners showed less penetration than 60 degree liners. One of the liners was annealed at 413°C for 20 hours and was fired at the optimum standoff for a 60 degree liner; this showed a slight increase in penetration.

Figure 7 (Table 11):

Yellow brass gave greater penetration than all other liners tested. Liners having 42, 55, and 75 degree apex angles when fired at the best standoff for the 60 degree liners gave less penetration than the 60° liners. One of the 60 degree liners was annealed for 2 hours at 413°C. The annealed liner gave less penetration than the nonannealed liners. Maximum penetration was obtained at a standoff of 15.0 cm.

Three shots were fired in rhyolite and about 20.0 cm of penetration was observed at 10.0 cm standoff. The reliability of the penetration data obtained is questionable due to extensive fracturing of the target, due to the brittle nature of the rhyolite and microfractures present from the quarrying operations.

Figure 8 (Table 12): Penetration in granite by 60 degree monel liners.

Penetration from 42, 55, and 75 degree liners was less than that for 60 degree liners. One of the cones was annealed at 871°C for 2 hours. The annealed cone gave less penetration than the nonannealed cone. The low point is attributed to large quartz crystals in the target. The plot is somewhat similar to yellow brass with less scatter

than that for brass.

Figure 9 (Table 13): Penetration in granite by 60 degree Maraging Steel liners.

Best penetration was obtained at 10.0 cm. The 42, 55, and 75 degree liners gave less penetration than 60 degree liners. Since the penetration trend was not promising and this liner required significant machining time, no further tests were made.

Figure 10 (Table 14):

Fifteen shots were fired into granite using 42 degree copper liners. Some scatter was observed in the penetration data. It was thought that the scatter may be due to the flange at the end of the cone. To determine this the flange was removed from 5 cones. However, no significant change was observed. For this metal, penetration in granite seems to be less sensitive to standoff as compared to the other liners. The scatter in data was probably due to the variations in liner mass (46.8-49.5 gm) and imperfections in manufacture.

Figure 11:

The general trend for all the metals is similar, i.e., an increase in penetration with increase in standoff until a maximum is reached, followed by a decrease in penetration. Aluminum requires a greater standoff than all other metals tested. This may be due to the properties of the aluminum jet. It is suggested that in the case of aluminum the penetration is due to a particle jet rather than by a cohesive jet. Except for aluminum all the liners show greater penetration at about 2.5 to 3.5 cone diameters standoff. Aluminum requires a greater standoff, between 4.0 and 5.0 cone diameters. Except for aluminum 7075 (T-6) all

the annealed liners gave less penetration than nonannealed liners. The scatter in the penetration data was due to the anisotropic nature of the target.

The granite blocks had small joints and the grain structure was nonuniform. Testing with concrete had shown that joints have an effect on the penetration. The abnormally large penetration observed with copper liner (charge No. 107, penetration 24.5 cm) was probably due to microfractures in the granite from previous testing in this block. Normally precautions were taken to avoid this situation.

B. Effect of Annealing on Liner Metals:

Steel liners were investigated by the Eastern Laboratories of Dupont (23,24). These liners were annealed at 1000°F, 1250°F, and 1650°F. Jets from Armco iron liners were superior in penetrating metals than other alloys tested,

In this study only one cone of each metal was annealed (Table 15) to note the effect of annealing on penetration. Except for aluminum 7075 (T-6) all other jets showed a decrease in penetration (Figure 6).

Table 9

Penetration in Granite by 60° Aluminum 2011 (T-3) Liners.

Charge No.	Standoff cm	Standoff CD[+]	Penetration cm	Penetration CD[+]	E.R.[*] cm	H.V.[**] cc
56	15.0	3.0	10.3	2.06	***	-
60	17.5	3.5	13.0	2.60	2.5	85.1[++]
62	18.0	3.8	12.8	2.56	***	-
57	20.0	4.0	15.0	3.0	***	-
118	20.0	4.0	12.7	2.54	1.0	13.3
115	21.0	4.2	9.5	1.90	***	-
61	22.5	4.5	13.0	2.60	***	-
59	25.0	5.0	8.0	1.60	***	-
119	25.0	5.0	10.2	2.16	2.5	66.8[++]
58	27.5	5.5	13.0	2.60	2.0	54.5
116	30.0	6.0	8.8	1.76	***	-
120	35.0	7.0	9.2	1.84	2.0	38.5
A130	20.0	4.0	11.2	2.24	1.2	16.9

\+ = Cone diameters

* E.R. = Effective Hole radius

** H.V. = Hole volume

*** = Hole was shattered

++ = Conical crater with smooth walls

A = Annealed liner

Table 10

Penetration in Granite by 60° Aluminum 7075 (T-6) Liners.

Charge No.	Standoff cm	Standoff CD+	Penetration cm	Penetration CD+	E.R.* cm	H.V.** cc
54	15.0	3.0	10.0	1.40	1.40	29.3
89	17.5	3.5	11.2	2.24	0.90	8.5
55	20.0	4.0	12.5	2.50	***	
87	22.5	4.5	8.5	1.70	4.0	142.4++
83	25.0	5.0	13.0	2.60	4.0	217.8++
88	27.5	5.5	10.0	2.00	1.0	11.0
84	32.5	6.5	12.0	2.40	***	
90	35.0	7.0	9.8	1.96	2.0	41.0++
A131	22.5	4.5	13.7	2.74	0.8	9.2

\+ CD = Cone diameters

* E.R. = Effective hole radius

** H.V. = Hole volume

*** = Hole was shattered

++ = Conical crater with smooth walls

A = Annealed liner

Table 11

Penetration in Granite by 60^{o} Yellow Brass Liners

Charge No.	Standoff		Penetration		E.R.*	H.V.**
	cm	CD+	cm	CD+	cm	cc
98	5.0	1.0	13.0	2.6	***	-
99	10.0	2.0	13.0	2.6	1.4	26.7
48	12.5	2.5	16.5	3.3	0.8	11.1
100	15.0	3.0	17.4	3.5	1.7	52.7
103	17.5	3.5	14.5	2.9	1.0	15.2
101	20.0	4.0	10.8	1.16	0.7	5.54
104	5.0	1.0	12.2	2.40	0.7	6.26
A129	15.0	3.0	14.6	2.92	0.8	8.6

\+ = Cone diameters

* E.R.= Effective hole radius

** H.V.= Hole volume

*** = Hole was shattered

A = Annealed liner

Table 12

Penetration in Granite by 60° Monel Liners

Charge No.	Standoff cm	Standoff CD+	Penetration cm	Penetration CD+	E.R.* cm	H.V.** cc
63	5.0	1.0	12.0	2.4	***	----
64	12.5	2.5	13.5	2.7	1.5	31.8
67	15.0	3.0	13.0	2.6	1.0	13.6
65	17.5	3.5	17.0	3.4	1.8	57.7
66	20.0	4.0	9.0	1.8	4.0	150.8++
68	20.0	4.0	15.5	3.1	***	
69	25.0	5.0	14.1	2.82	1.0	14.8
A128	17.5	3.5	13.4	2.68	0.9	11.4

\+ CD = Cone diameters

* E.R. = Effective hole radius

** H.V. = Hole volume

*** = Hole was shattered

++ = Smooth wall conical crater

A = Annealed liner

Table 13

Penetration in Granite by 60° Maraging Steel

(Vascomax 250) Liners

Charge No.	Standoff cm	Standoff CD+	Penetration cm	Penetration CD+	E.R.* cm	H.V.** cc
39	5.0	1.0	14.5	2.90	2.0	60.74++
40	10.0	2.0	16.0	3.20	1.5	37.7
41	15.0	3.0	10.0	2.00	4.0	167.5++

\+ CD = Cone diameters

* E.R. = Effective hole radius

** H.V. = Hole volume

++ = Smooth wall conical crater

Table 14

Penetration in Granite by 42° Copper Liners

Charge No.	Standoff cm	Standoff CD+	Penetration cm	Penetration CD+	E.R.* cm	H.V.** cc
106	5.0	1.0	14.5	2.90	1.1	18.4
108	10.0	2.0	13.5	2.70	0.9	11.5
107	15.0	3.0	24.5	4.90	1.2	36.9
110	20.0	4.0	11.0	2.20	0.6	4.2
112	15.0	3.0	10,2	2.04		
109	25.0	5.0	12.5	2.5	0.8	8.4
124	5.0	1.0	10.6	2.42	0.9	9.0
125	15.0	3.0	13,2	2.64	0.8	8.8
126	17.5	3,5	10.0	2.00		
128	25.0	5.0	14.8	2.96	0.85	11.2
-145	5.0	1.0	10.0	2.00	1.00	10.5
-146	10.0	2.0	13.6	2.72	1.00	14.2
-147	15.0	3.0	14.3	2.86	1.00	15.0
-148	17.5	3.5	10.8	2.16	1.1	13.7
-149	22.5	4.5	13.2	2.64	1.1	16.7
A127	16.25	3.25	14.1	2.82	0,9	12.0

\+ CD = Cone diameters
* E.R. = Effective hole diameter
** H.V. = Hole volume
\- = Copper liners without flange
A = Annealed liner

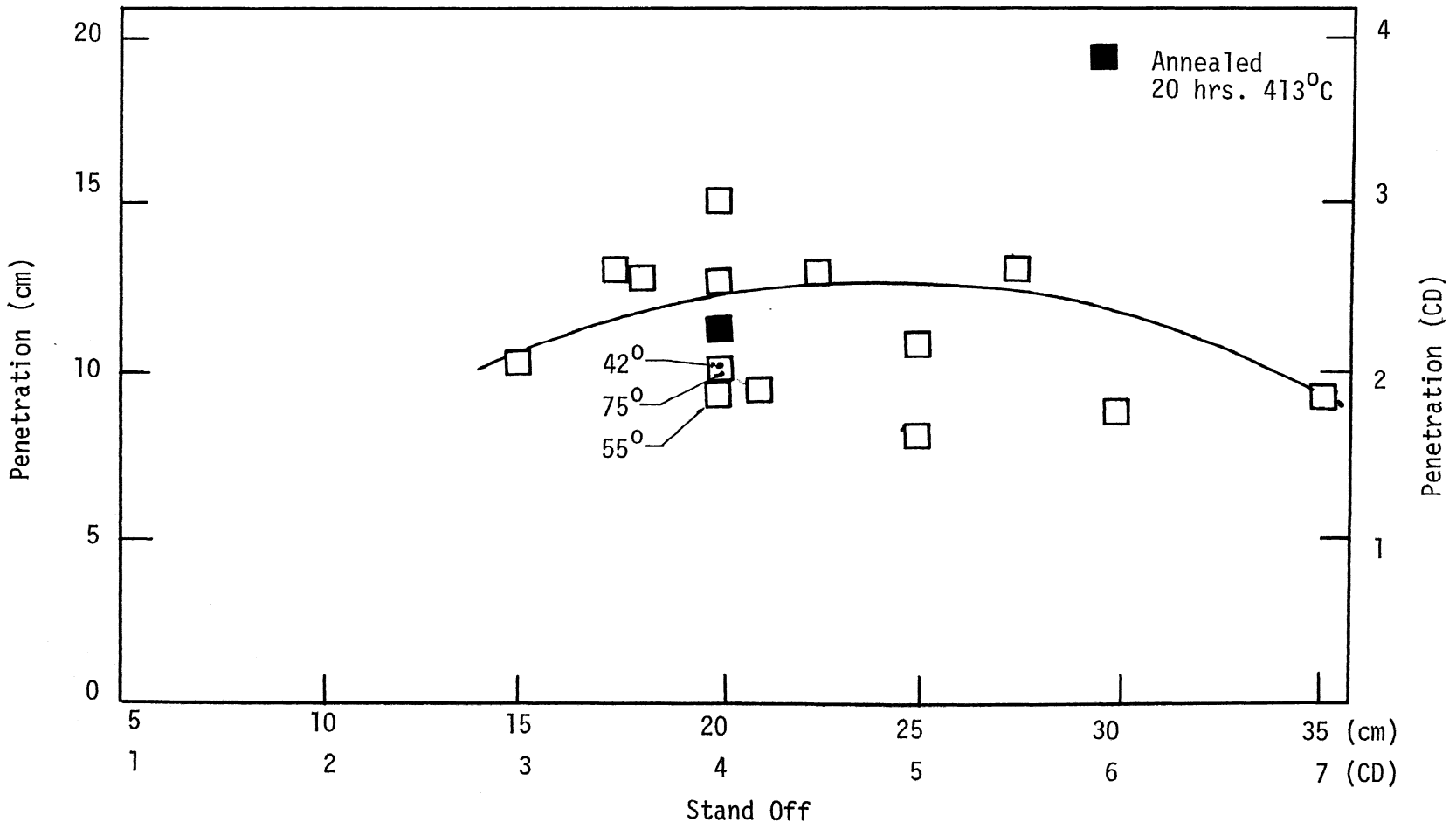

Figure 5. Penetration in Missouri Red Granite by 60 Degree Aluminum 2011 (T-3) Liners

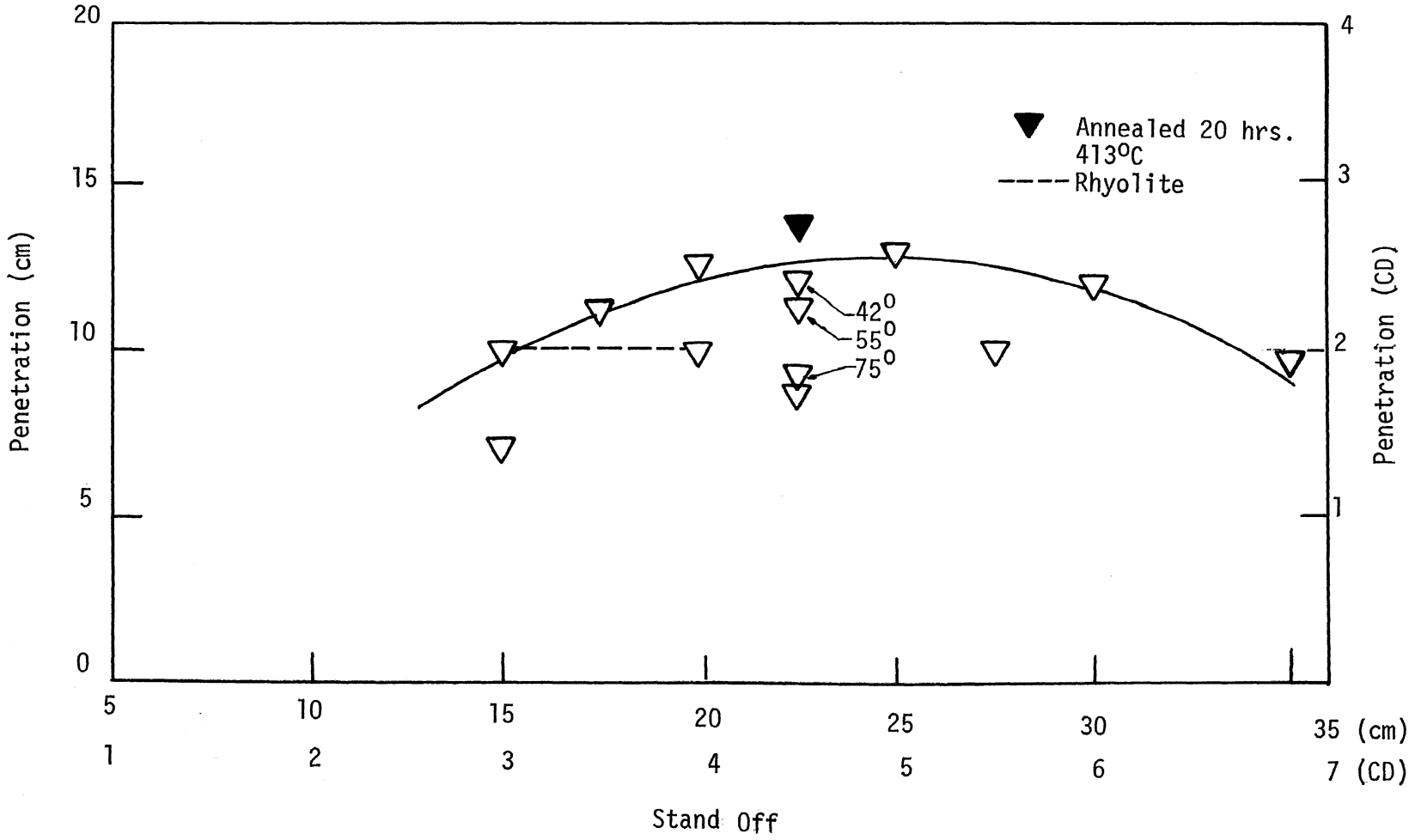

Figure 6. Penetration in Missouri Red Granite by
60 Degree Aluminum 7075 (T-6) Liners

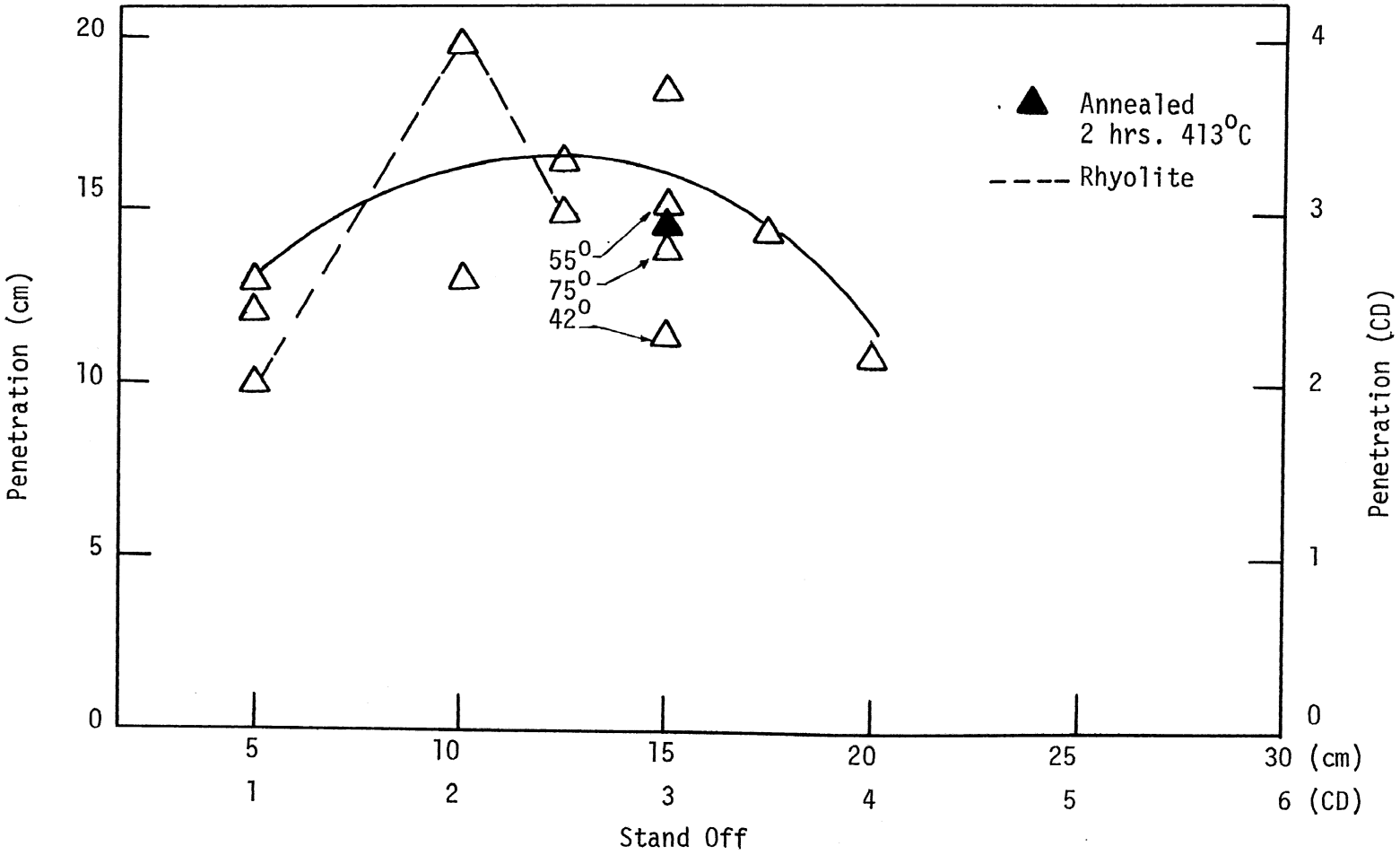

Figure 7. Penetration in Missouri Red Granite by
60 Degree Yellow Brass Liners

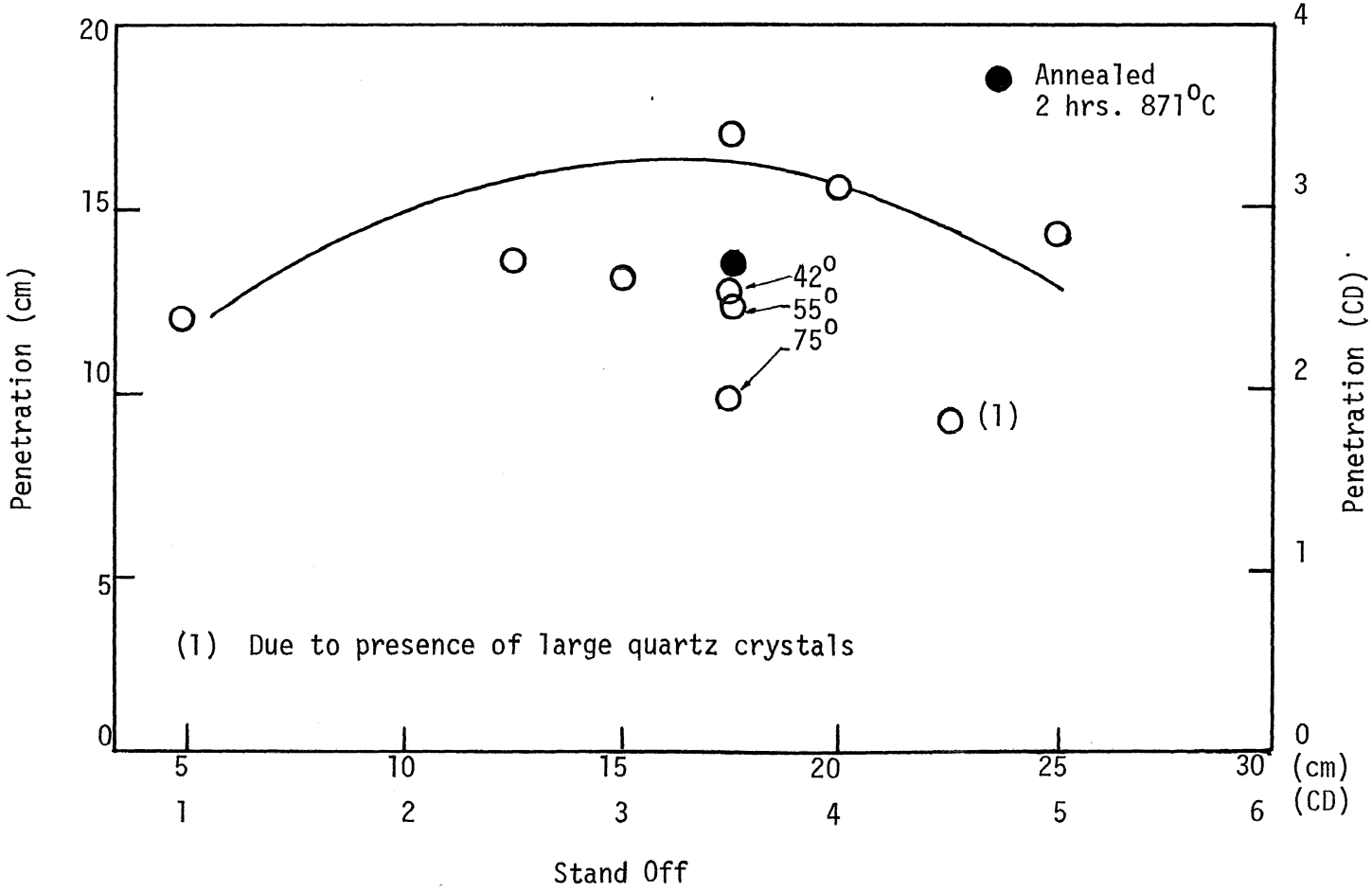

Figure 8. Penetration in Missouri Red Granite by
60 Degree Monel Liners

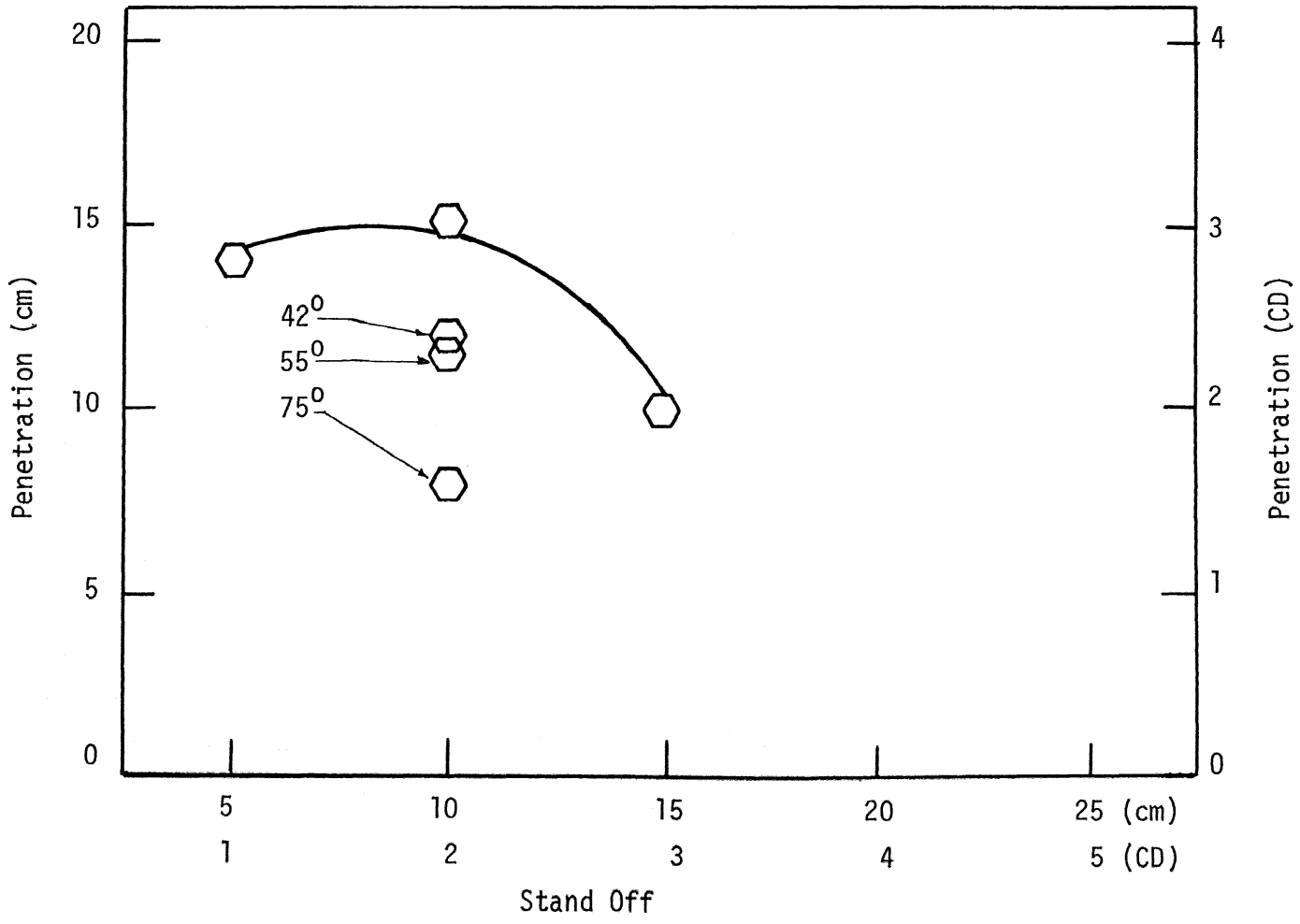

Figure 9. Penetration in Missouri Red Granite by 60^{o} Maraging Steel Liners

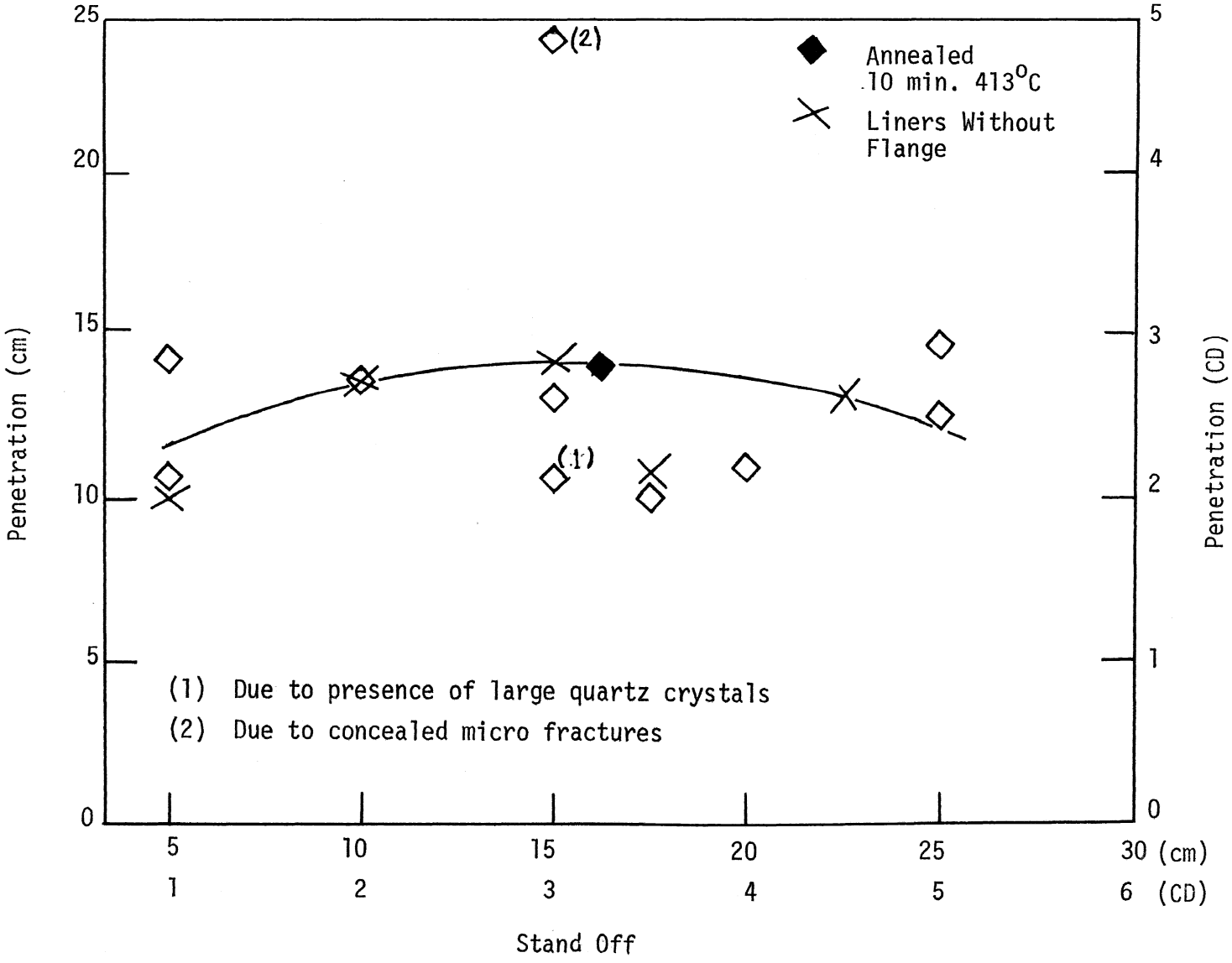

Figure 10. Penetration in Missouri Red Granite by 42° Copper Liners

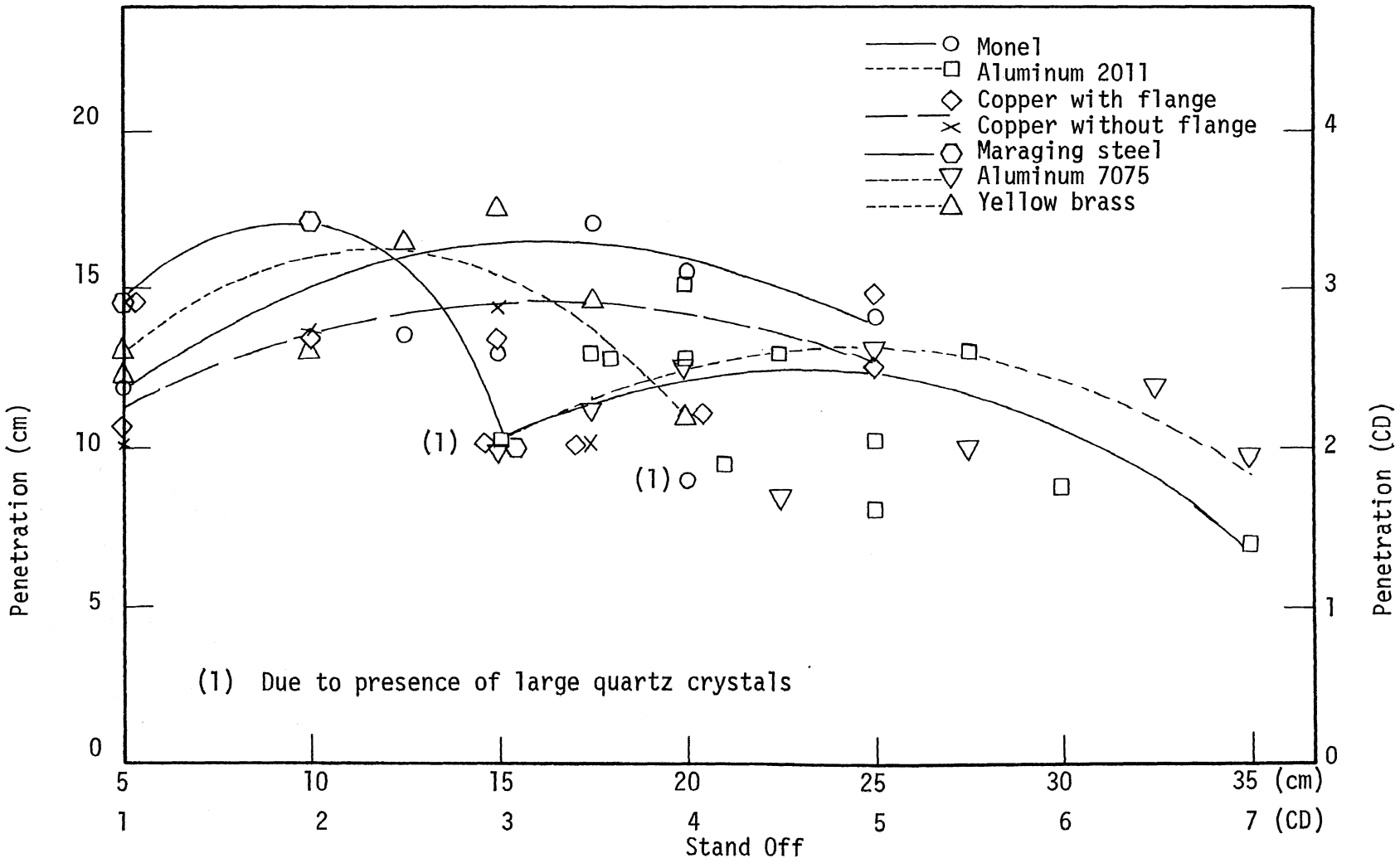

Figure 11. Penetration in Granite by Various Liners Tested

Table 15

Annealing Data

Metal	Hardness as rec'd	Hardness after annealing	Annealing Time Hrs.	Annealing Temp. ^{o}C
Aluminum 7075 (T-6)	63 RE	72 RE	20	413
Aluminum 2011 (T-3)	95 RE	52 RE	20	413
Monel	96 RB	52 RB	2	871
Yellow Brass	84 RK	74 RK	2	413
Copper	34 RE	29 RE	1/6	413
Maraging Steel (Vascomax 250)	29 RC	(Not Annealed)		

C. Jet Characteristics and Jet Tip Velocity:

Attempts were made to photograph jets moving through air and helium atmospheres (Figure 12). The jet was visible for the first few microseconds, then the interactions between the shock waves created by the jet tip obscured it.

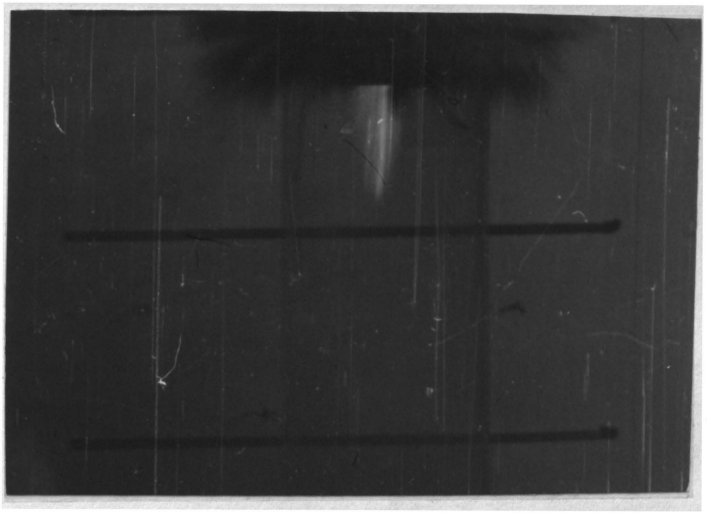

Figure 12. Shaped Charge Jet 26 Microseconds after Initiation

Flash X-ray equipment used by several investigators (2, 18, 25) has shown that jets are continuous and cohesive for a short time. Subsequently the jet breaks up into small particles of approximately the same length.

On the basis of published data (14, 15), it is estimated that the jets formed in this investigation remain continuous for the following approximate times:

Aluminum	40-55 μsecs
Copper	50-60 μsecs
Monel	50-60 μsecs
Steel	50-60 μsecs
Yellow Brass	50-60 μsecs

Pin oscilloscope techniques were employed to obtain jet tip velocities through air and granite. Two shots per metal were fired to obtain the rate of penetration and jet tip velocity. The jet tip velocity through air is given below:

Aluminum 2011 (T-3)	8.09 mm/ μsec
Aluminum 7075 (T-6)	7.91 mm/ μsec
Copper	8.87 mm/ μsec
Monel	9.83 mm/ μsec
Steel	7.69 mm/ μsec
Yellow Brass	8.87 mm/ μsec

Penetration velocity or rate of penetration through granite was obtained by placing pin sets into the granite slabs. The velocity decreases rapidly in the first few centimeters (Figure 13) and then

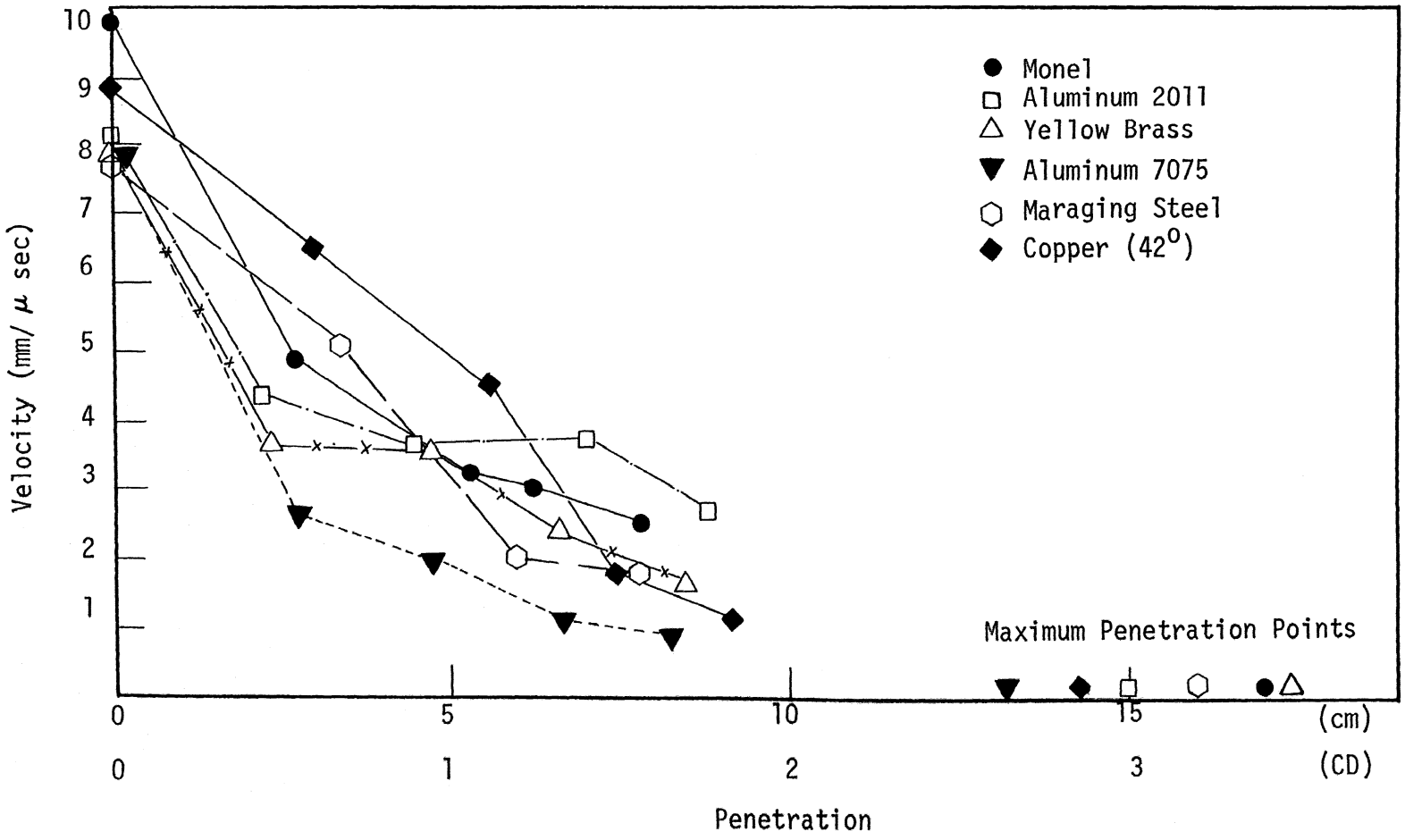

Figure 13. Jet Tip Velocity Through Granite Blocks

decreases slowly until maximum penetration is achieved.

D. Mechanics of Penetration:

Penetration involves shock compression of the materials to very high pressure, possibly accompanied by some melting and vaporization of the target material. This motion involves both extremely high stresses and strains. The final phase of the hole formation involves ejaculation of the fine material from the hole.

A shock receding into the oncoming jet will actually be carried below the original target surface when the jet velocity exceeds the velocity of the shock wave generated in the jet (Figure 14). This critical velocity is a function of the densities and the compressibilities of the jet and target material.

As the jet continues to penetrate, the shock wave into the target precedes the jet-target interface. Rarefaction from the free surface of the target and the jet modify the shock system and the shock becomes conical inside the target. To eliminate the shorting out of the pinsets by the shockwaves rather than by the jet, during rate of penetration measurements, the target was placed inside a sand filled container.

If the shock in the jet is carried below the original target surface, then the jet material which has not yet been reached by the shock is carried well into the target and one may expect a greater penetration. On the other hand, if the shock in the jet recedes above the target surface, the sides of the shock zone in the jet are unsupported and increased lateral flow may be expected, with shallower craters. Such craters were observed in the case of aluminum liners.

Figure 14. Detonation front and associated shock wave 52 μ sec after initiation

Target Effect:

The manner in which rock behaves under jet impact has not yet been fully explained. It is a phenomenon that still requires additional study.

Bowden (22) has suggested that five different forms of deformation take place in the target material when subjected to large impact pressure by water jets: circumferential surface fractures, subsurface flow and fracture, large scale plastic deformation leading to permanent deformation, shear deformation around the periphery of the impact zone, and failure due to reflection of stress waves.

In general the fractures observed in Missouri red granite were composites of all these types. Attempts were made to observe the development of fractures in the target by the jet (Figure 1C). The rarefaction of the shock waves formed a luminous ionized zone (Figure 14). No fractures in the targets were visible up to 52 microseconds after initiation. These fractures were developed due to the pressure exerted by the jet on the rock. The fractures propagate in a radial manner from the center of the hole suggesting failure due to tension. Fracturing continued beyond the jet termination point in concrete blocks. These fractures are due to an intense pressure pulse passing over the target. The target being unable to deform relieves stress by fracturing subsurfaces.

Figure 15: Fracture pattern in granite

These fractures were developed due to the pressure exerted by the jet on the rock. The fractures propagate in a radial manner from the

hole, suggesting failure due to tension and compression.

Figure 15. Fracture pattern in granite

Figure 16: Fracturing continued beyond the jet termination point in the concrete blocks. These fractures are due to an intense pressure pulse passing over the target. The target being unable to deform relieves stress by fracturing subsurfaces..

Figure 17: A longitudinal section of the hole in granite. The target material in direct line of the jet was under great stress due to the pressure exerted by the jet. The rock surrounding the hole was highly fractured and powdery and indicated the flow of the material in line with the jet direction.

E. Slug formation and Metallographic observations:

As the liner begins to collapse due to the detonation pressure (Figure 1) the inner wall of the liner moves toward the cone axis at a greater speed than the outer wall. This causes a redistribution of the

Figure 16. Subsurface fractures in concrete

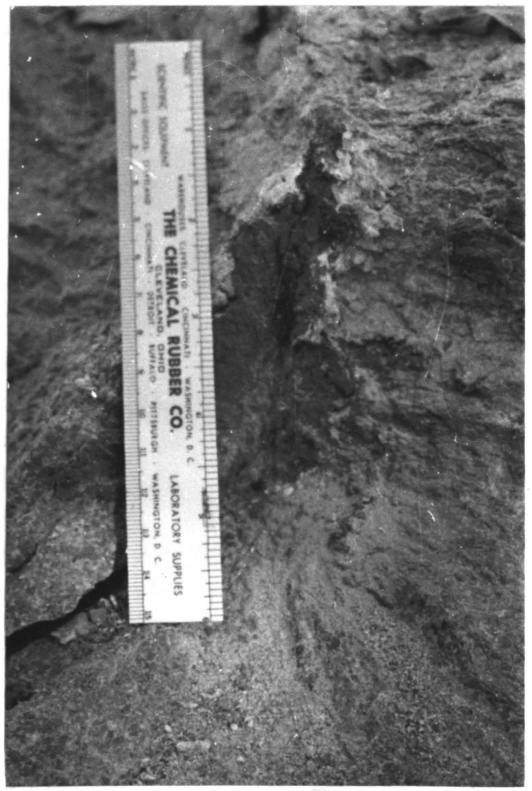

Figure 17. Longitudinal section of the shaped charge hole

liner mass leading to fast jet formation from the inner wall and slow jet or slug formation from the outer wall. Attempts were made to observe the cone collapse by viewing it through a mirror and utilizing the framing camera. Figure 18 shows the cone reflected in a mirror with the conical grid and the development of the shock front. The outer wall of the liner collapses toward the cone axis forming a solid conical slug.

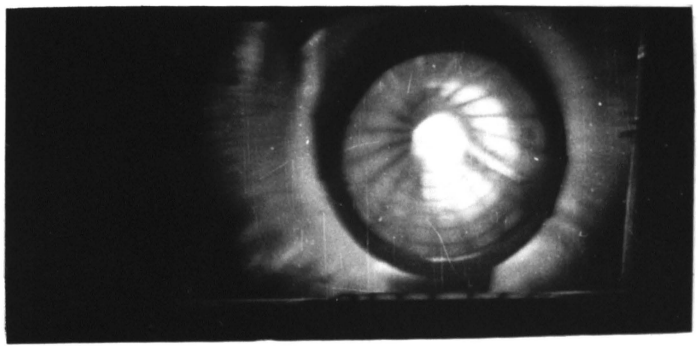

Figure 18. Framing Camera Record of Cone Collapse

Slugs from yellow brass were smaller than the others. No slugs were recovered from Aluminum 7075. A carefully designed experiment was performed to collect slugs from aluminum liners. A slug was obtained for Aluminum 2011. It is suggested that zinc is responsible for small or no slug formation. Metallography was performed on the slugs and metals used for this investigation (Appendix D). The following conclusions were drawn from the metallographs:

1) In all cases the grains have elongated and are oriented along the normal to the slug's longitudinal axis.
2) The grains in the slug are smaller than those in the metal. In all cases the size of the grains had reduced by at least 1/10

of the original grain size.

3) The grain size is smallest near the axis of the slug and increases in size to the edge of the slug.
4) In all of the slugs a pin hole or fracture was observed at the center of the transverse axis.
5) Except in the case of copper and possibly aluminum no evidence of melting was present. Some of the material from the bottom of the hole was analyzed microscopically. This revealed spherical inclusions indicating melting of copper particles. These particles might have been from the particle jet (Figure 19).
6) There was some indication of recrystallization and twinning.
7) The hardness of the slugs had decreased in aluminum 2011 and brass, suggesting an annealing effect. In monel and steel the hardness increased, suggesting some degree of precipitation. No evidence of the precipitation was visible through optical microscopy.
8) There was no significant change in the densities of the metal forming the slugs.

F. Nature of Holes in Granite:

A great deal of communition was observed. Spallation was always present around the collar of the hole. The rock immediately around the hole was crushed and friable. Figure 20 shows the highly fractured granite with metal inclusions.

All of the holes were coated with jet material. Each hole had various

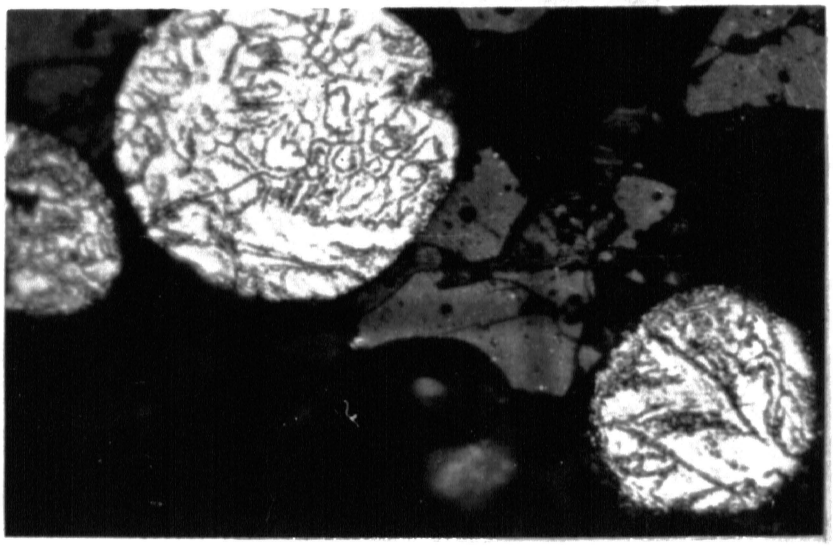

Figure 19. Photomicrograph of Copper imbedded in granite

x250

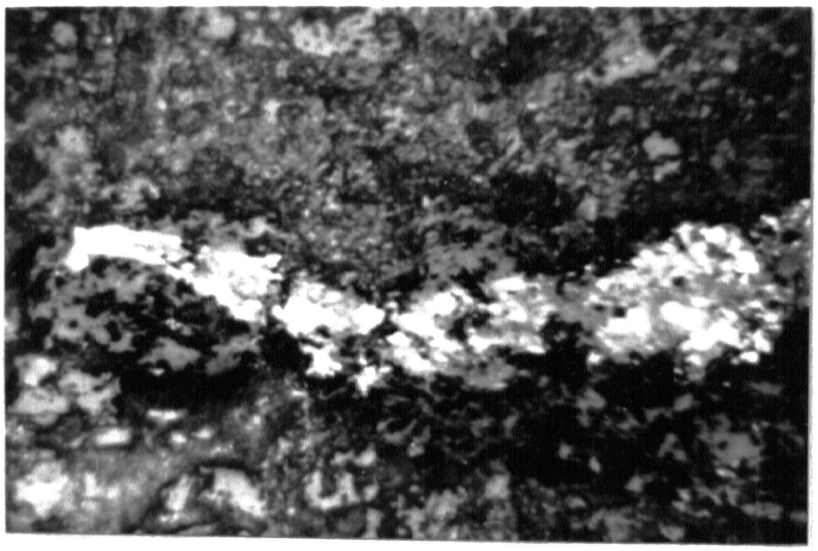

Figure 20. Photomicrograph of steel inclusion of inner wall of a hole in the granite

x250

colorations depending upon the liner metal. In the case of brass the holes were brick red in color while for copper the holes were red. Aluminum, monel, and steel gave black coloration.

In all cases metal from the jet had deposited at the end of the hole in a fan shape. Four types of holes were formed. These holes are shown in Figure 21. Type (d) had very smooth walls and they were discolored due to air blast. Some of the holes contained spherical globules indicating melting. However, except for one case (Figure 19) melting was not evidenced by optical microscopy. In some instances there was evidence of jet material intruding into the rock.

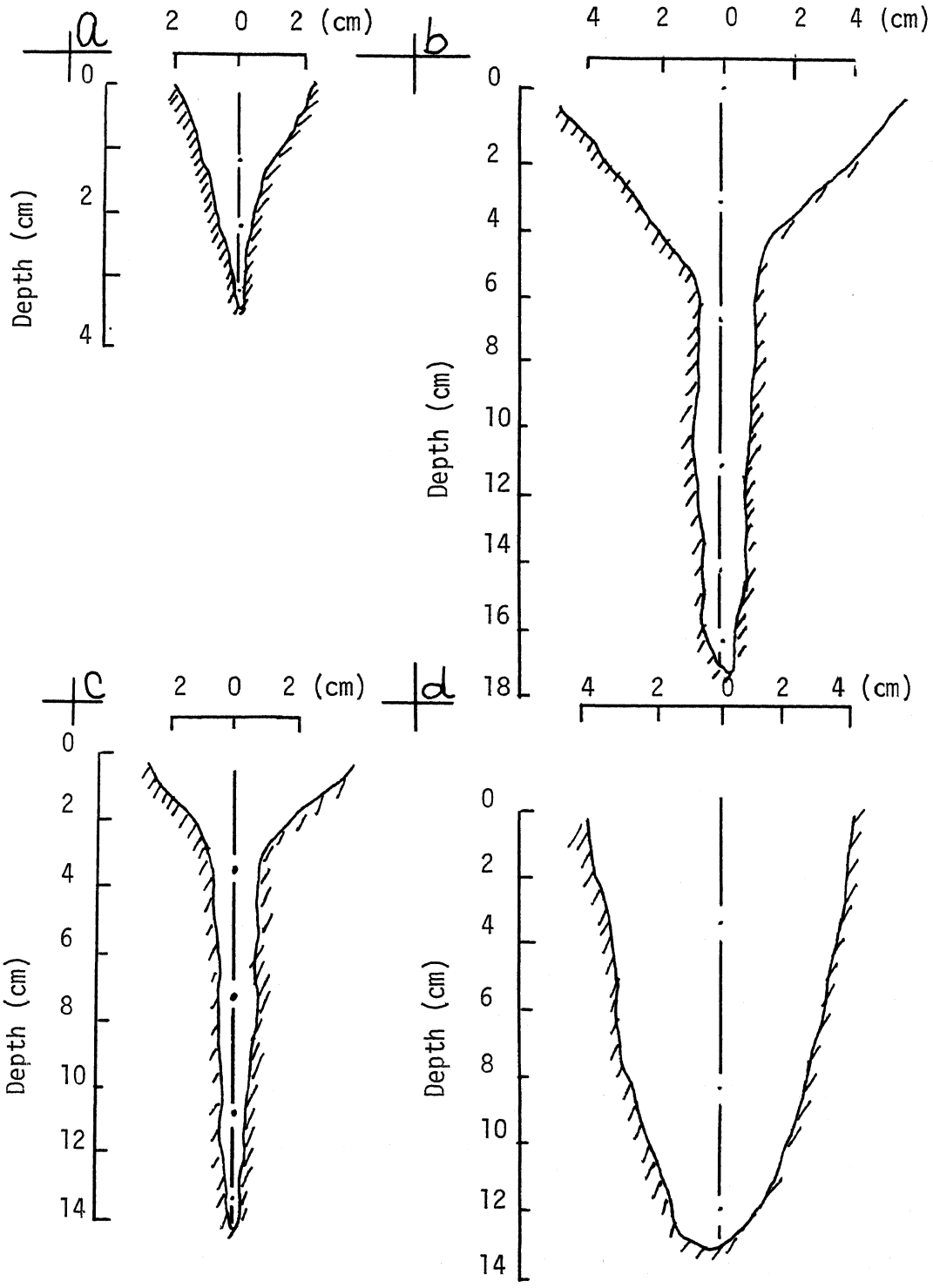

Figure 21. Typical hole profiles in granite

V. SUMMARY, CONCLUSIONS, AND RECOMMENDATIONS

1. Jets from the 60 degree monel, brass, and steel liners gave the deepest penetration. Monel required greater standoff than brass and steel but less than aluminum.
2. Copper and brass liners gave equal penetration for 42 degree apex angles.
3. Aluminum liners were easier to machine than other liner metals. Maraging steel and the monel liners were the most difficult to fabricate.
4. Except for aluminum 7075 it appears that annealing has no effect on penetration.
5. Aluminum 7075 jets gave greater penetration than aluminum 2011.
6. Jets from 60 degree liners containing zinc produced small slugs or none at all.
7. The holes in the granite were uniform and approximated right circular cones. About 3-4 cm of the hole was removed by spalling and blast effects.
8. Fractures in granite due to the jet and blast were caused by compression, tension, and shear failure. Rock in the direct line of the jet was highly crushed and shredded and the jet material had intruded into the rock matrix.
9. Framing camera photography was inadequate to define jet characteristics in air although in an inert atmosphere it was possible to see the jet for a few microseconds. Metallic probes were used to obtain jet tip velocity and rate of penetration through granite

slabs using a pin oscilloscope.

10. Metallographic studies indicated a symmetrical liner collapse. The grains were highly fractured and the hardness had decreased in brass and aluminum. Some evidence of melting of the metal was present, and a phase transition was suspected in steel liners. The density of the slugs and liners remained essentially constant.
11. A three-dimensional expression (Equation 3) was developed to describe the collapse time for conical liners. For an assumed constant collapse velocity the calculated stagnation point velocity was almost constant.
12. Penetration parameters for granite could not be calculated from equations 4-7 due to inadequate information about the jet characteristics.

Recommendations:

1. An investigation should be initiated to obtain the jet characteristics and the minimum penetration velocities for different rocks. This information may be used to modify equations 4 through 7.
2. The three-dimensional theory should be verified using flash x-ray equipment.
3. Employing equations 4-7 and the three-dimensional collapse theory, a computer program may be developed to evaluate shaped charge performance of different liners in rocks.
4. A full scale investigation should be initiated to employ shaped charges for drilling and blasting of hard rocks.
5. A more detailed metallurgical investigation should be undertaken to determine the behavior of liners under high pressures.

APPENDIX A

List of Symbols

CR	Cone radius
CD	Cone diameter
d	Wall thickness of cone
h	Height of the cone
H_{lim}	Limiting value of charge length
H.V.	Hole volume
L	Length of the jet
m	Mass per unit length
m_e	Mass of the liner element
P	Penetration
P_T	Total penetration
P_{max}	Maximum penetration
r_j	Radius of the jet
S	A point between S_2 and S_3
S_2	Normal distance to axis from inner wall of cone
S_3	Normal distance to axis from outer wall of cone
$\dot{S}$	Initial collapse velocity
S_{3i}	Initial value of S_3
SO	Stand off
T	Kinetic energy of collapse

t_1	Jet breakup time
t_c	Collapse time of liner
U_D	Detonation velocity of explosive
U^{min}	Minimum penetration velocity of target
V_j	Jet velocity
V_c	Collapse velocity of liner
V_j^o	Jet tip velocity
Z_o	Distance from virtual origin (assumed point of origin of jet) to the target surface
α	Half apex angle
β	Collapse angle
γ	$\sqrt{\rho_t/\rho_j}$
$\Delta 1$	Length of element along the slant height of cone
λ	Correction factor for discontinuous jet
ρ_t	Density of target
ρ_j	Density of jet

APPENDIX B

Derivation of Collapse Time and Kinetic Energy Expressions.

The following assumptions were used in the development of the expressions presented in the text to obtain liner collapse time and the kinetic energy of collapse:

1. Metal under high pressure and impulsive load is considered to be an incompressible fluid.
2. Collapse is normal to the slant height of the cone.
3. The collapse velocity is constant.

Consider a section of the cone and an element on the surface having a small length along the slant height of the cone to be $\Delta 1$. For this $\Delta 1$ the element will have a small surface area and a volume. Figure 2 shows the cone collapse dimensions. From this

$$r_2 = S_2 \text{ Cos } \alpha$$

$$r_3 = S_3 \text{ Cos } \alpha$$

the volume of this element

$$V_e = 1/2\Delta 1 \rho \pi \text{Cos}\alpha (S_2^2 - S_3^2) \qquad (1)$$

If the volume of the element remains constant then

$$V_e = \text{constant}$$

and therefore

$$(2V_e/\pi \text{Cos}\alpha \Delta 1) = (S_2^2 - S_3^2)$$

will be conserved as the liner is collapsing. Differentiating $(S_2^2 - S_3^2)$ with respect to time

$$2S_2\dot{S}_2 = 2S_3\dot{S}_3 = 2S\dot{S}$$

for any value of S, thus

$$\dot{S}_3 = (S\,\dot{S} / S_3) \quad (2)$$

The kinetic energy (T) of the element is given by

$$T = 1/2\Delta l\rho \int_0^{2\pi\cos\alpha} \int_{S_3}^{S_2} d\theta S \; dS \; (dS/dt)^2$$

$$= \Delta l\rho\pi\cos\alpha \int_{S_3}^{S_2} S \; (S\, dS/dt)^2 \; 1/(S^2) \; dS$$

$$= \Delta l\rho\pi\cos\alpha \; (S_3\dot{S}_3)^2 \int_{S_3}^{S_2} (1/S) \; dS$$

$$T = \Delta l\rho\pi\cos\alpha \; (S_3 \dot{S}_3)^2 \; \ln (S_2/S_3) \quad (3)$$

From Equation (3) $\dot{S}_3$ can be obtained and is given by

$$\left[dS_3/dt\right]^2 = \left(\dot{S}_3\right)^2 = \left[\frac{T}{\Delta l\rho\pi\cos\alpha S_3^2 \; \ln \; S_2/S_3}\right]$$

Therefore

$$dt = \left[\frac{\Delta l\rho\pi\cos\alpha S_3^2 \; \ln \; S_2/S_3}{T}\right]^{\frac{1}{2}} dS_3 \quad (4)$$

Integrating Equation (4) for t gives

$$\int_0^t dt = (\rho\pi\Delta l\cos\alpha/T)^{\frac{1}{2}} \int_{r_j}^{S_{3i}} S_3 \; (\ln S_2/S_3)^{\frac{1}{2}} \, dS_3$$

Therefore

$$t_c = (\rho\pi\Delta l \ \mathrm{Cos}\alpha/T)^{\frac{1}{2}} \quad 1/2 \int_{r_j/\mathrm{Cos}\alpha}^{S_{3i}} S_3 \ln\left(\frac{S_3 + d}{S_3}\right) dS_3$$

APPENDIX C

Instrumentation

Explosive phenomenon occur too rapidly to permit detailed observations by ordinary means. The detonation velocities are usually expressed in mm/microsecond. The instruments used in microtime physics must be capable of rendering clear information related by some definite time scale to the explosive reaction. In general, these instruments can be divided into two groups:

1. Optical systems and
2. Electronic systems.

1. Optical Systems:

Those that make a single exposure of extremely short duration at some instant during the process of initiation and those that capture all or most of the record continuously or intermittently.

For this investigation a framing camera (Cordin model 1011) was used. It is capable of taking pictures at the rate of 1.25 million frames per second on 35 mm film thus giving an interframe time of 0.8 microseconds. The following shaped charge parameters were investigated using this instrument:

1. Development of detonation front with respect to shaped charge design,
2. Determination of liner collapse velocity,
3. Determination of Jet characteristics, and
4. Jet effect on target.

While it was possible to obtain the mimimum shaped charge length necessary, it was not possible to obtain jet characteristics or collapse

velocity. Interference from the shockwaves created a highly luminous front obscuring the view. It was possible to see the jet for a few microseconds in inert atmosphere, but the photographs were not satisfactory (Figure 12).

The behavior of Granite blocks and Concrete blocks under jet impact was observed (Figure 1C and 14). No movement was seen in the targets.

It is suggested that for future investigations, the target and the charge should be enclosed in an inert atmosphere.

2. Electronic Systems:

Several techniques are available to measure explosive velocity using electronic methods. The object is to externally trigger an oscilloscope and record the trace generated. This trace can be calibrated to obtain a time-distance plot and hence velocity. Techniques available at the Research Center employ a specially designed plug-in-unit (Cordin 135 to be used with modified Tecktronics 535 A). It consists of a bank of electronically charged pins connected to the oscilloscope. This method was found quite suitable for measuring jet tip velocity and rate of penetration through granite blocks.

Jet tip Velocity:

Two shots per metal were fired. The charges were mounted on long (5.08 cm inside diameter) plastic tubes. Pins were fabricated from 0.3 mm aluminum shim stock metal. These pins were spaced 5.0 cm apart and insulated by thin plastic. The first pin was used to trigger the oscilloscope, and the velocity of the jet tip was obtained from the oscilloscope trace.

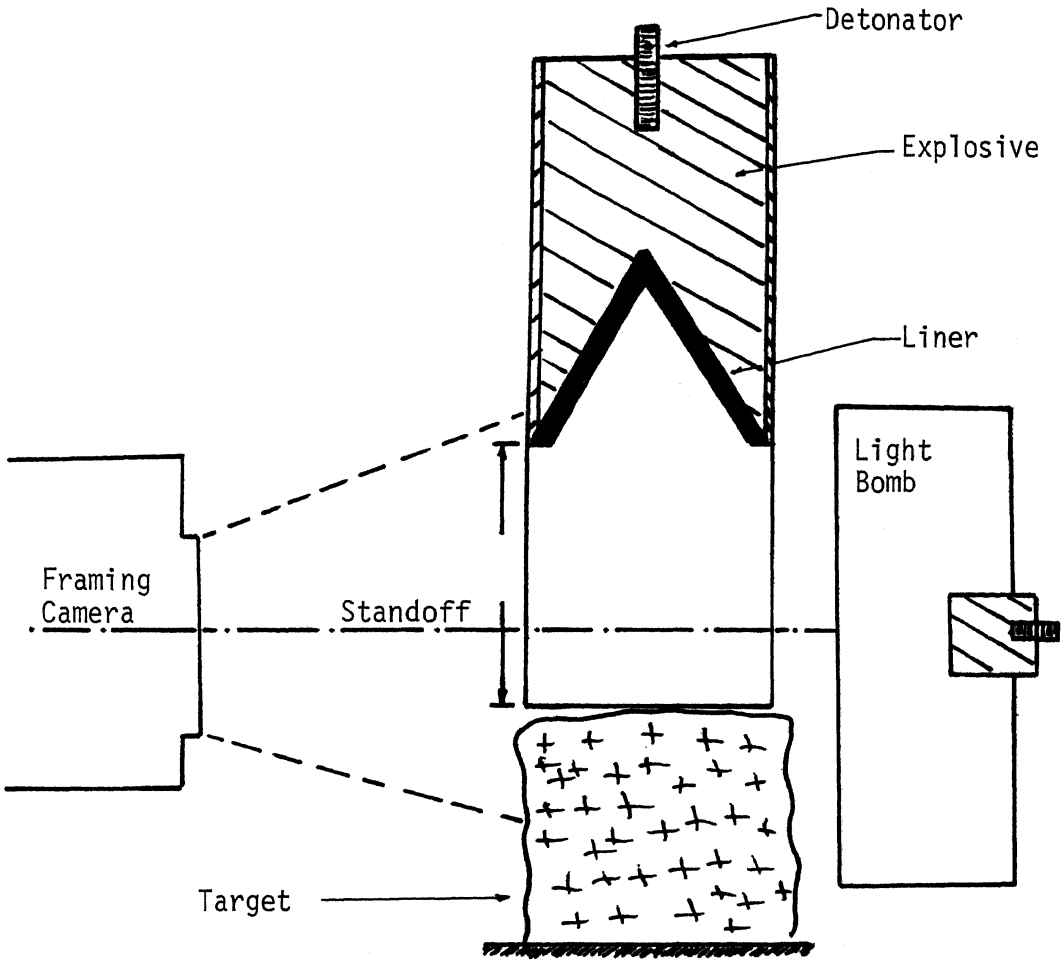

Figure 1C. Arrangement to Photograph Jet Characteristics and Target Response

Rate of Penetration:

In order to measure the rate of penetration in granite, 10 cm slabs varying in thickness from 1.5 cm to 3.5 cm were stacked together with the pins inserted between them. The first pin was used to trigger the oscilloscope.

There were two types of experimental difficulties:

1. Those which can effect the magnitude but not the reproducibility, and
2. Those which effect the reproducibility.

1. This difficulty is due to the interference of the shock waves generated by the explosive and the jet (Figure 14). These shock waves can short the pins giving erroneous results. To prevent this, the targets were placed inside a sand filled container and the pins were insulated with plastic.

Despite this precaution some scatter was observed. These variations are attributed to the interfaces between the granite slabs. Jet tip velocity was more reproducible than the rate of penetration and was essentially constant over the distance tested.

2. There are many factors which affect the reproducibility and are inherent in explosive research. Some of these are: flatness of the slabs, planarity of the jet, change in pin location due to transportation, etc. Care was taken to minimize these problems.

APPENDIX D

Metallography of the Metals and Slugs

The changes in microstructure following explosive impact and flow are primarily in the distribution density of lattice defects such as dislocations, vacancies, interstitials, stacking faults, mechanical twins, and an amount of strain induced transformation in alloys normally susceptible to such transitions (26). The large amount of energy imparted to the liners by explosives causes a severe deformation and reduction in size of the grains. A systematic metallographic investigation was made to observe the effect of high pressure generated by Composition C-4 on the liners.

A representative sample was taken from each of the metals used to fabricate the cones. Samples were prepared for metallographic analysis employing standard procedures (27).

The slugs were cut and mounted in a manner to reveal the structure along the longitudinal as well as the transverse axis. The greatest deformation was near the center of the slug. The grains showed a flow in the direction of the metal toward the stagnation point. In some cases fracture at the stagnation zone was observed. Metallographs are presented in Figures 1D-16D.

Figure 1D: Metallograph of aluminum 2011 (T-3). This alloy has a face centered cubic lattice structure. It is a free machining alloy. Grain boundaries are well defined and are equiaxed.

Figure 2D: Metallograph of aluminum 2011 slug. The grains are highly fractured and are about 1/150th of the original grain size.

Some recrystallization is indicated. Fine grains are almost equiaxed. A fracture was seen along the transverse axis of the slug near the stagnation axis. The hardness of the metal had decreased from 63 RB to 21 RB.

Figure 3D: Metallograph of aluminum 7075 (T-6). This is an aluminum zinc alloy. No slug was recovered in this case. The α grains are well defined and are equiaxed. Mostly α grains with some black inclusions and boundary precipitation can be seen.

Figure 4D: Metallograph of yellow brass. The α grains are white and occupy about 90 percent of the area of the specimen. The grains are well defined and are equiaxed.

Figure 5D: Metallograph of the brass slug taken along the longitudinal axis near the edge of the slug. The grains are fractured and show elongation along the slug axis. The β particles had elongated near the center of the slug and were highly fractured. The flow of the particles was along the transverse axis of the slug. The hardness had decreased from 73 RB to 53 RB suggesting some annealing effects.

Figures 6D, 7D and 19: Metallographs of the copper metal, slug, and a photomicrograph of a copper particle imbedded in granite. In Figure 6D annealing twins are visible. The grains are well defined and are equiaxed. Figure 7D shows the structure of the slug along the longitudinal axis of the slug. No fractures were visible but a pin hole was observed at the center of the slug. The grains are well defined and are equiaxed. The size of the grains is about 1/10th of the original grains. Grains are elongated along the direction of flow. No melting was observed. The grains are completely crushed. Recrystallization after deformation is apparent. Figure 19 is a photomicrograph

of the metal particles and highly fractured granite from the end of the hole. Some melting of the metal is evidenced. The hardness of the slug had increased from 34 RE to 14.5 RB.

Figure 8D: Metallograph of monel which shows a roughly equiaxed grain of β phase containing annealing twins and no second phase. Small amounts of an unidentified second phase inclusion are seen.

Figures 9D, 10D, and 11D: Figure 9D is a metallograph of a monel slug taken along the longitudinal axis. The grains are highly deformed and have elongated along the direction of flow. Heavy deformations and flow patterns are clearly visible. Black inclusions of a second phase are lenticular in shape. Figure 10D shows the structure of the slug at the center. The stagnation point has a large crack and small fractures in a radial pattern. Figure 11D shows the crack at the center surrounded by very fine recrystallized grains, several orders of magnitude smaller than the original grains, gradiating up to 10 percent of the original metal grains. The hardness of the slug had increased from 12.5 RC to 21 RC.

Figures 12D and 13D: Metallographs of maraging steel (Vascomax 250). The grain boundaries are well defined and the grains are equiaxed. Annealing twins are visible. Figure 13D was taken at the edge of the transverse axis of the slug. White lines are fractures while the black area is unidentified.

Figure 14D: A sketch of the steel slug showing variations in hardness. The outer edge of the metal was fractured. These fractures extend toward the center in a conical pattern.

Figures 15D and 16D: Metallographs of the structure at the edge of the steel slug along the longitudinal axis and at the center

of the slug. No microstructure is visible at this magnification. Some phase transformation is suspected. The grains increase in size away from the center. The hardness of the slug had increased from 28.5 RC to 36.75 RC (average), suggesting some degree of precipitation. It was not possible to see precipitates by optical microscopy.

Table 1D

Etchants used for Metallography

Metal	Etchant	Etchant Composition		Remarks
Aluminum 2011, 7075 and slug	Keller's etch	HF (conc.) HCl (conc.) HNO_3 (conc.) H_2O	1.0 ml 1.5 ml 2.5 ml 95.0 ml	Swabbed for about 30 seconds.
Copper Brass and their slugs	Ferric Chloride	$FeCl_3$ Ethyl Alcohol HCl	5.0 gm 95.0 ml 2.0 ml	Swabbed for about 40 seconds
Monel Slugs	Nitric Acid	HNO_3 Ethyl Alcohol (95%)	2.0 ml 100.0 ml	Immersed for 60 seconds
Maraging Steel and slugs	Mixed acids	HCl HNO_3 $CuCl_1$ H_2O	50.0 ml 25.0 ml 1.0 gm 150.0 ml	Swabbed for 60 seconds

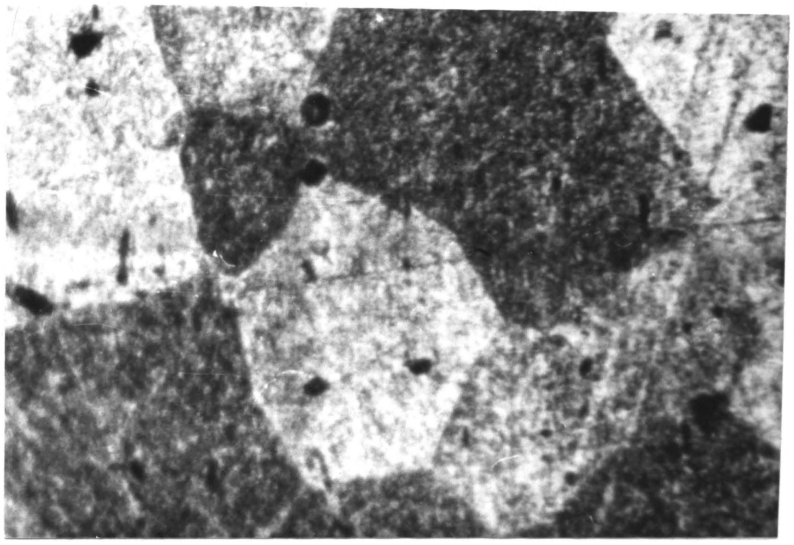

Figure 1D. Metallograph of Aluminum 2011

x250

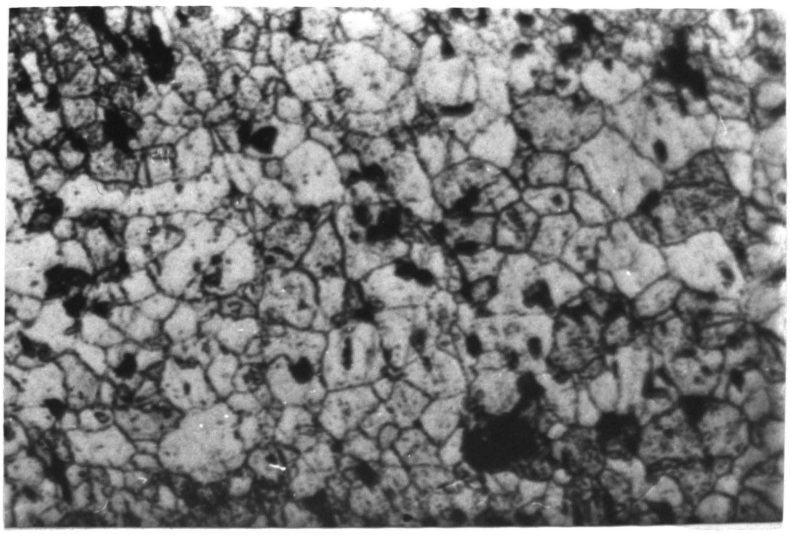

Figure 2D. Metallograph of Aluminum Slug

x250

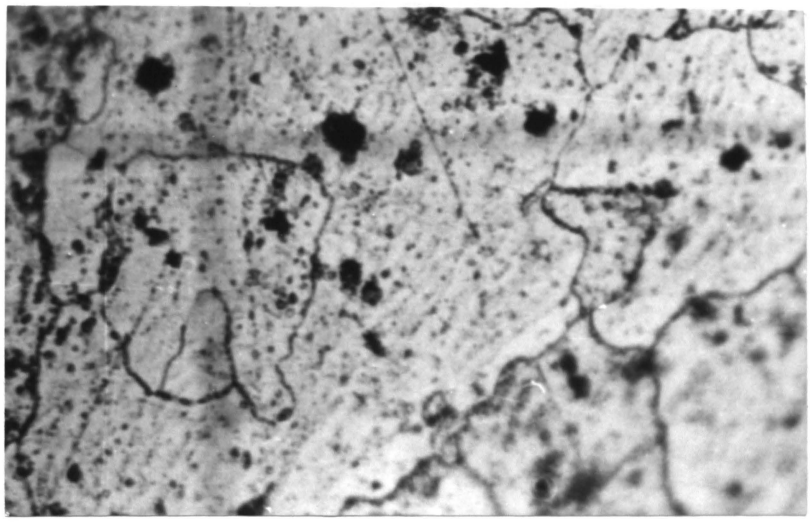

Figure 3D. Metallograph of Aluminum 7075

x250

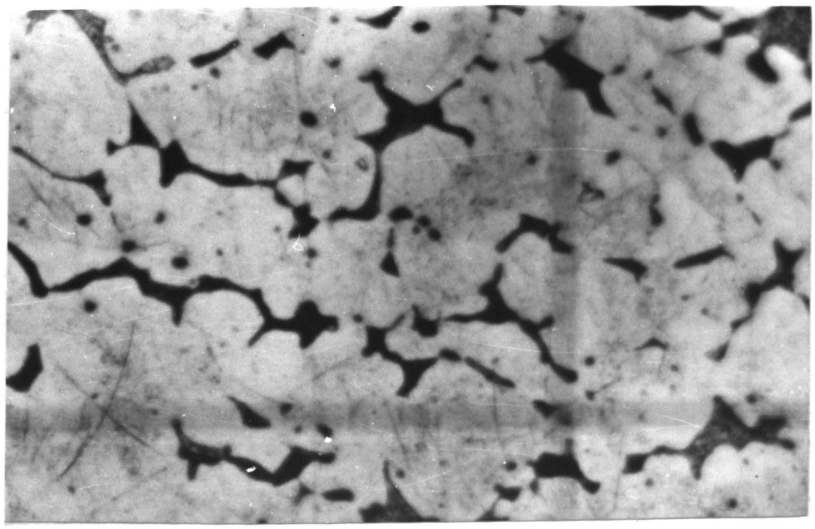

Figure 4D. Metallograph of Yellow Brass

x250

Figure 5D. Metallograph at the side of slug, yellow brass
x250

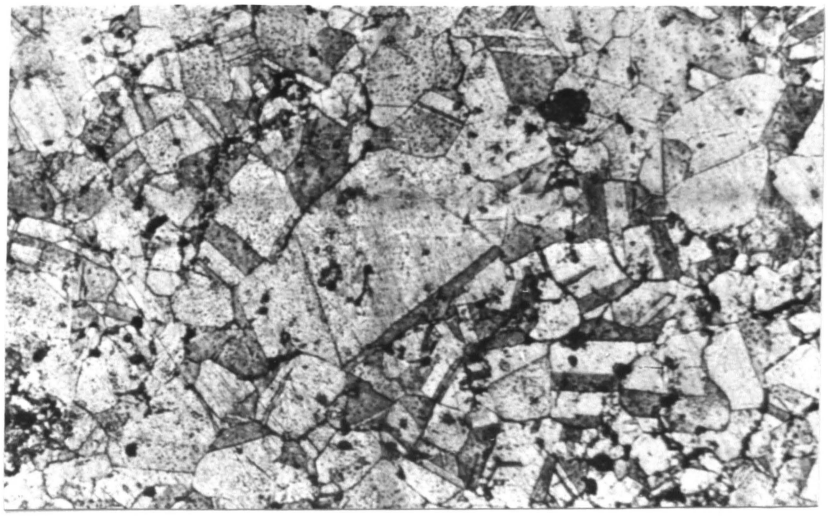

Figure 6D. Metallograph of Copper
x250

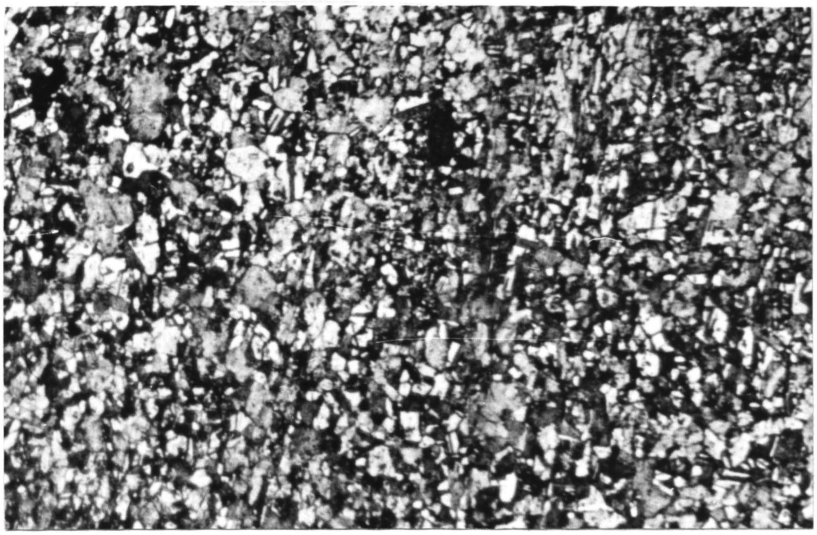

Figure 7D. Metallograph of Copper Slug

x250

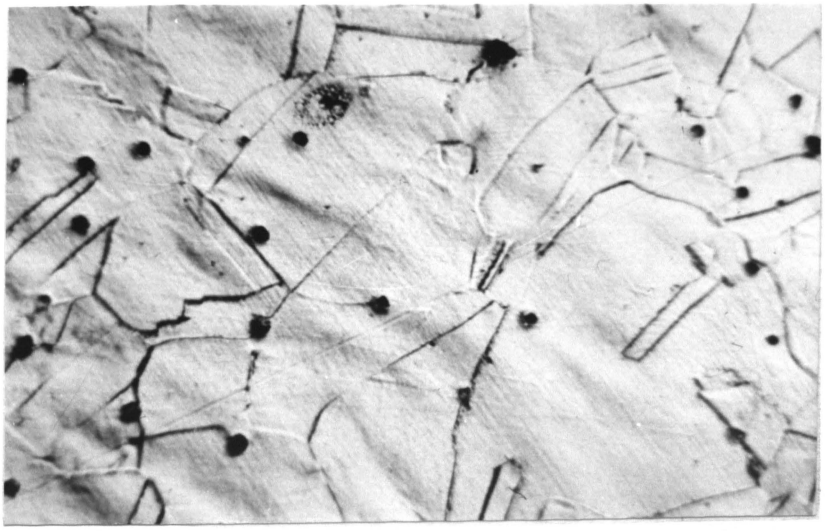

Figure 8D. Photomicrograph of Monel

x250

Figure 9D. Photomicrograph of Monel Slug. Taken along the transverse axis.

x250

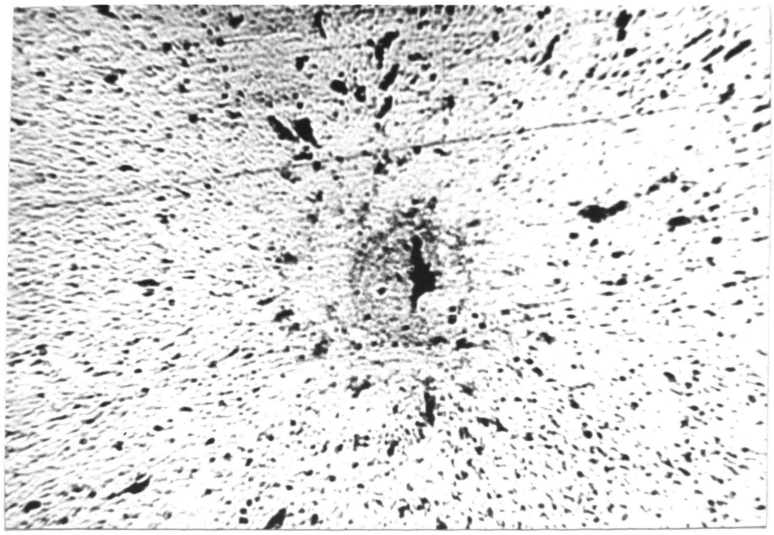

Figure 10D. Metallograph of the Center of the Slug, Monel.

x250

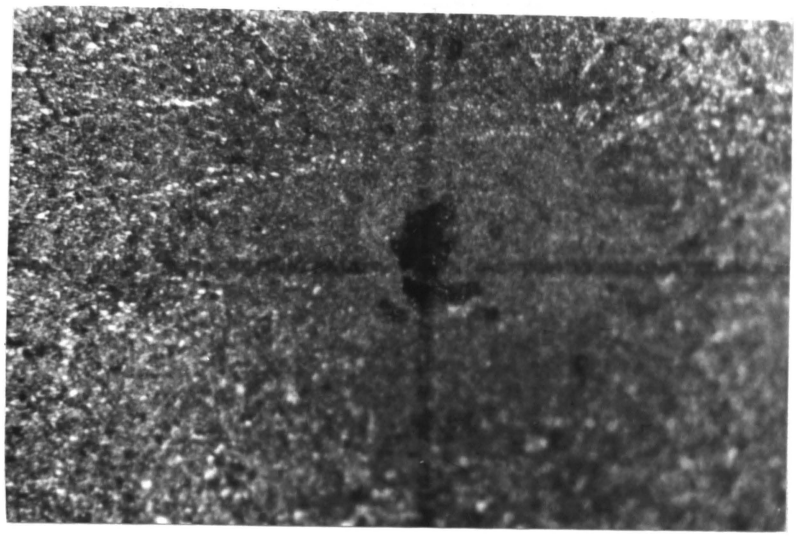

Figure 11D. Metallograph of Monel Slug along the transverse axis. Recrystallization near the center can be seen.

x250

Figure 12D. Metallograph of Steel

x250

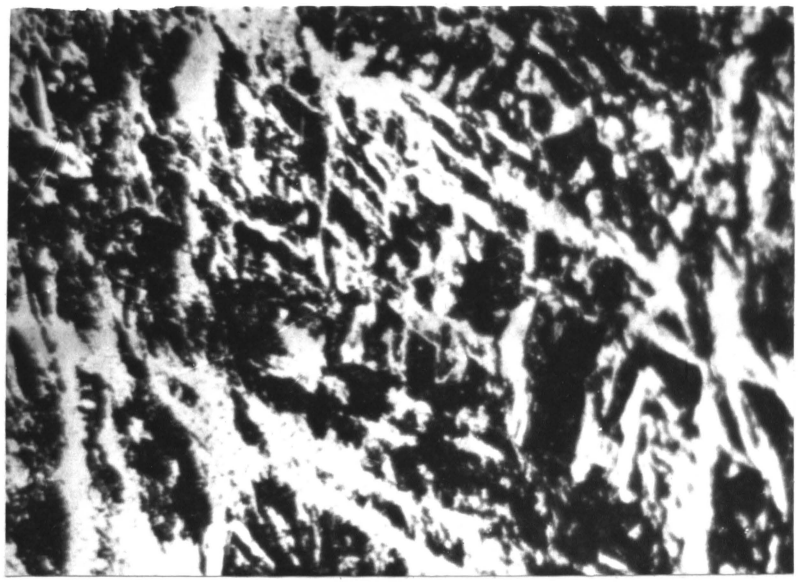

Figure 13D. Metallograph of Steel Slug

x250

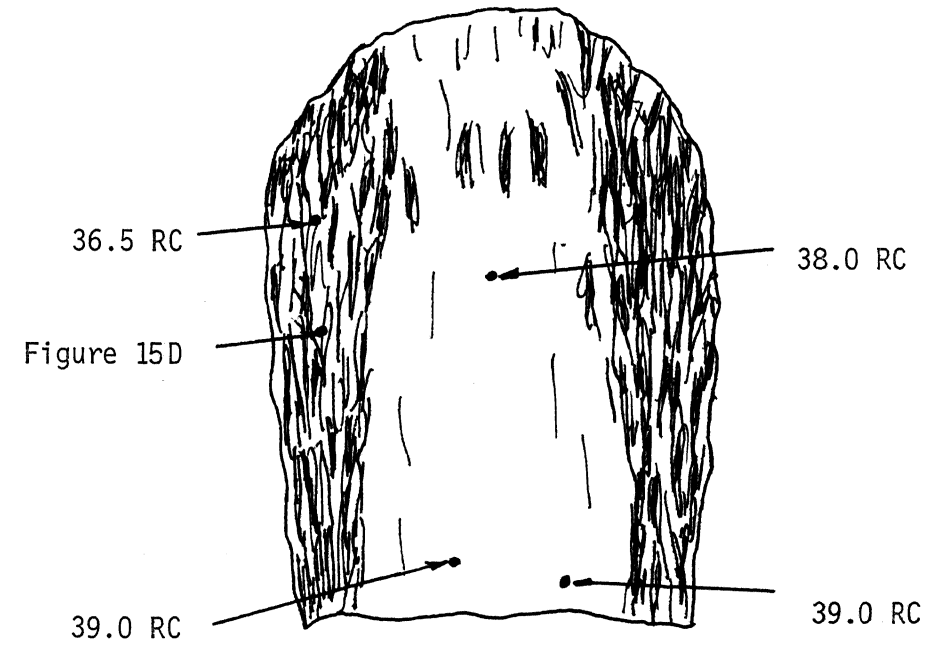

LONGITUDINAL SECTION

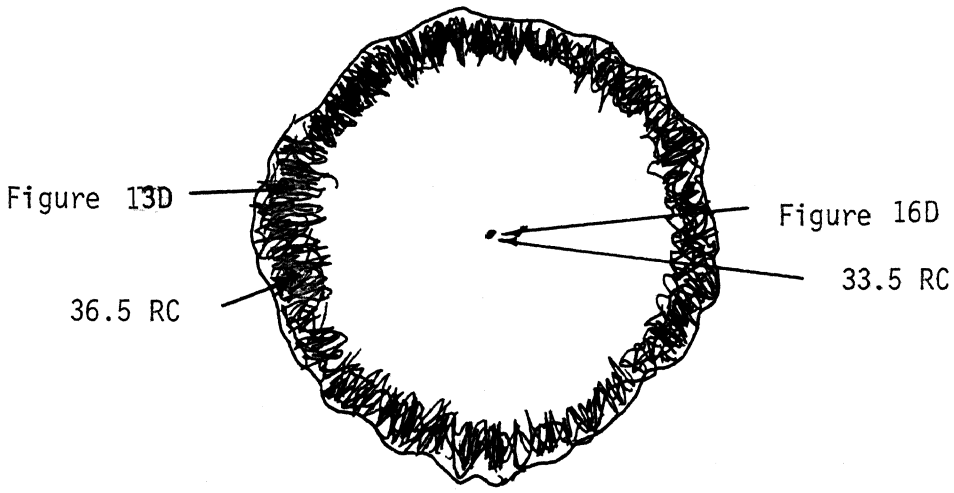

TRANSVERSE SECTION

Figure 14D. Steel Slug and its Hardness

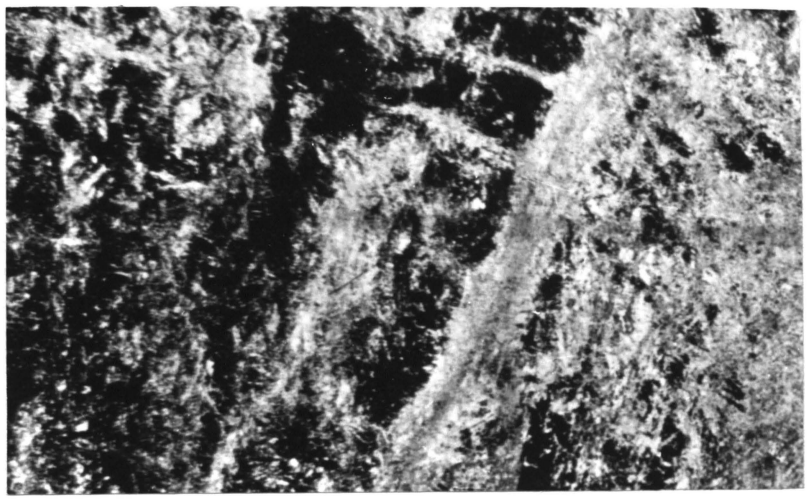

Figure 15D. Metallograph of Maraging Steel Slug at Edge of Slug

x250

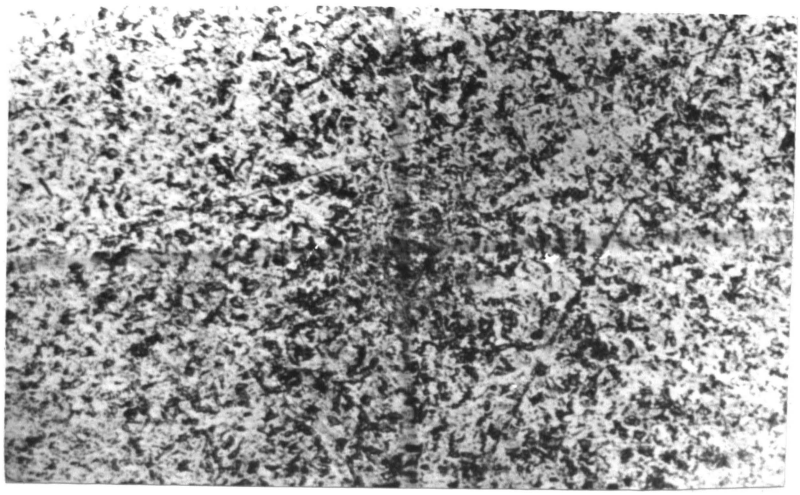

Figure 16D. Metallograph taken at center of Slug

x250

REFERENCES

1. Birkhoff, G., MacDougal, D. P., Pugh, E. M., and Sir Taylor, G., "Explosives with Lined Cavities", Journal of Applied Physics, (1948), Vol. 19, 563-582.

2. Baum, F. A., Stanykovich, R. P., and Shekter, B. I., Physics of an Explosion, (AD 400 151), New York, Research Information Service, (1949), 546.

3. Eichelberger, R. J., "Re-Examination of the Theories of Jet Formation and Target Penetration by Lined Cavity Charges", Ph.D. dissertation, Carnegie Institute of Technology, Pittsburgh, (1954).

4. Clark, G. B., "Studies of the Design of Shaped Charges and Their Effect in Breaking Concrete Blocks", American Institute of Mining Engineers, Technical Paper 2157, (1947)

5. Austin, F. C., "Lined-Cavity Charges and Their use in Rock and Earth Materials", New Mexico Institute of Technology, Bulletin 69, (1959).

6. Huttl, J. B., "The Shaped Charge for Cheaper Mine Blasting", Engineering and Mining Journal, (1946), Vol. 147, 58-63.

7. Hill, R., Mott, H. F., and Pack, D. C., "Penetration by Munroe Jets", Ministry of Supply, A. C. No. 5756, HMSO, London, January, (1944).

8. Pack, D. C., and Evans, W. M., "Penetration by High Velocity Munroe Jets-I", Proceedings of the Physical Society of London, (1951), Section B, Vol. 64, 298.

9. Pack, D. C., and Evans, W. M., "Penetration by High Velocity Munroe Jets-II", Proceedings of the Physical Society of London, (1951), Section B, Vol. 64, 303.

10. Pugh, E. M., Eichelberger, R. J., and Rostoker, N., "Theory of Jet Formation by Charges with Lined Conical Cavities", Journal of Applied Physics, (1952), Vol. 23, 532.

11. Sterne, T. E., "A Note on Collapsing Cylindrical Shells", Journal of Applied Physics, (1950), Vol. 21, 73-74.

12. Eichelberger, R. J., "Prediction of Shaped Charge Performance from Release Wave Theory", Transactions of the Symposium on Shaped Charges, BRL 909 (AD 58 899), Aberdeen Proving Grounds Maryland, (1953), 192.

13. Jackson, R. F., "The Problem of Lagrange for Shaped Charge Liner Collapse", Transactions of the Symposium on Shaped Charges, BRL 909 (AD 58 899), Aberdeen Proving Grounds, Maryland, (1953), 131.

14. Dipersio, R., Simon, J., and Merendino, A. B., "Penetration of Shaped Charge Jet into Metallic Targets", BRL 1296 (AD 476 717), Aberdeen Proving Grounds, Maryland, (1965).

15. Allison, F. E., and Vitali, R., "A New Method of Computing Penetration Variables by Shaped Charge Jets", BRL 1184 (AD 400 485), Aberdeen Proving Grounds, Maryland, (1963).

16. Klamer, O. A., "Shaped Charge Scaling", AD 600 273, Picatinny Arsenal, Dover, New Jersey, (1964).

17. Zernow, L., and Simon, J., "High Strain Plasticity of Liner Metals and Jet Behavior", Transactions of the Symposium on Shaped Charges, BRL 909 (AD 58 899), Aberdeen Proving Grounds, Maryland, (1953), 107-130.

18. Rinehart, J. S., and Pearson, J., Behavior of Metals Under Impulsive Loads, New York, Dover Publications, (1965), 203.

19. Brimmer, R. A., "Manual for Shaped Charge Design", Navord Report 1248 (ATI 84 949), China Lake, California, (1950).

20. Winn, H., "The Present Status of the Artillery Ammunition Program at the Firestone Tire and Rubber Company", Transactions of the Symposium on Shaped Charges, BRL 909 (AD 58 899), Aberdeen Proving Grounds, Aberdeen, Maryland, (1953), 25.

21. Brown, J., Personal Communication.

22. Bowden, F. P., Brunton, J. H., "The Deformation of Solids by Liquid Impact at Supersonic Speeds", Proceedings of the Royal Society of London, (1961), Series A, Vol. 263, (1961), 433.

23. E. I. Dupont and Co., "Investigation of Cavity Effect", Final Report, E. I. Dupont De Nemours and Co., Wilmington, Delaware, (1943).

24. E. I. Dupont and Co., "Evaluation of Deep Drawing Steels for Manufacture of Purity Charge Cones", E. I. Dupont De Nemours and Co., Wilmington, Delaware, (1944).

25. Clark, J. C., "Flash Radiography Applied to Ordinance Problems", Journal of Applied Physics, (1949), Vol. 20, 363-370.

26. Orava, R. N., and Otto, H. E., "The Effect of High Energy Rate Forming on Terminal Characteristics of Metal-A Review", Journal of Metals, (February 1970), 17-30.

27. Kehl, G. H., Principles of Metallographic Laboratory Practice, 3rd Edition, New York, McGraw-Hill Co., (1944).

VITA

Hemendra Nath Kalia was born on February 11, 1939, at Amritsar, Punjab, India. He received his primary and secondary education in India. He graduated with a diploma in mining engineering, receiving honors in mining machinery from Wigan and District Mining and Technical College, Wigan, Lancashire, England. He received his M.S. in mining from the University of Missouri-Rolla in May 1967.

The author has 5 years experience in various phases of mining operations. He is an associate member of the Institution of Mining Engineers, London, and the Association of Mining, Electrical and Mechanical Engineers, Manchester and is a member of Sigma Gamma Epsilon. He was awarded First Class Certificate of Competency in coal, ironstone, fireclay and shale mining by the Ministry of Power, England, on February 1965.

Since June 1968, he has been associated with Rock Mechanics and Explosive Research Center as senior research assistant.